105
5-17-82

dr. 609

MASTER

SERI/PR-9233-1-T2
(DE82013338)

INVESTIGATION OF PHOTOVOLTAIC MECHANISMS IN POLYCRYSTALLINE THIN-FILM SOLAR CELLS

Interim Technical Report for the Period November 1, 1980—July 31, 1981

By
T. A. Temofonte
J. R. Szedon
T. W. O'Keeffe

March 5, 1982

Work Performed Under Contract No. AC02-77CH00178

Westinghouse R&D Center
Pittsburgh, Pennsylvania

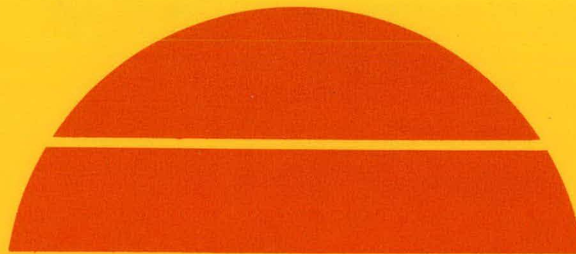

U.S. Department of Energy

Solar Energy

DISCLAIMER

This report was prepared as an account of work sponsored by an agency of the United States Government. Neither the United States Government nor any agency Thereof, nor any of their employees, makes any warranty, express or implied, or assumes any legal liability or responsibility for the accuracy, completeness, or usefulness of any information, apparatus, product, or process disclosed, or represents that its use would not infringe privately owned rights. Reference herein to any specific commercial product, process, or service by trade name, trademark, manufacturer, or otherwise does not necessarily constitute or imply its endorsement, recommendation, or favoring by the United States Government or any agency thereof. The views and opinions of authors expressed herein do not necessarily state or reflect those of the United States Government or any agency thereof.

DISCLAIMER

Portions of this document may be illegible in electronic image products. Images are produced from the best available original document.

DISCLAIMER

"This report was prepared as an account of work sponsored by an agency of the United States Government. Neither the United States Government nor any agency thereof, nor any of their employees, makes any warranty, express or implied, or assumes any legal liability or responsibility for the accuracy, completeness, or usefulness of any information, apparatus, product, or process disclosed, or represents that its use would not infringe privately owned rights. Reference herein to any specific commercial product, process, or service by trade name, trademark, manufacturer, or otherwise, does not necessarily constitute or imply its endorsement, recommendation, or favoring by the United States Government or any agency thereof. The views and opinions of authors expressed herein do not necessarily state or reflect those of the United States Government or any agency thereof."

This report has been reproduced directly from the best available copy.

Available from the National Technical Information Service, U. S. Department of Commerce, Springfield, Virginia 22161.

Price: Printed Copy A04
Microfiche A01

Codes are used for pricing all publications. The code is determined by the number of pages in the publication. Information pertaining to the pricing codes can be found in the current issues of the following publications, which are generally available in most libraries: *Energy Research Abstracts, (ERA); Government Reports Announcements* and Index (*GRA* and I); *Scientific and Technical Abstract Reports (STAR);* and publication, NTIS-PR-360 available from (NTIS) at the above address.

SERI/PR-9233-1-T2
(DE82013338)
Distribution Category UC-63

INVESTIGATION OF PHOTOVOLTAIC MECHANISMS IN POLYCRYSTALLINE THIN-FILM SOLAR CELLS

T. A. Temofonte, J. R. Szedon, and T. W. O'Keeffe

Interim Technical Report
November 1, 1980 - July 31, 1981

Contract No. XG-0-9233-1

March 5, 1982

Solar Energy Research Institute
Golden, CO 80401

Westinghouse R&D Center
1310 Beulah Road
Pittsburgh, Pennsylvania 15235

THIS PAGE

WAS INTENTIONALLY

LEFT BLANK

TABLE OF CONTENTS

		Page
	ABSTRACT	iv
	LIST OF FIGURES	v
	LIST OF TABLES	viii
1.	SUMMARY	1
2.	INTRODUCTION	5
	2.1 Contract Objective	5
	2.2 Approach	5
	2.2.1 Task 1: Modelling	5
	2.2.2 Task 2: Measurement Techniques Development	5
	2.2.3 Task 3: Grain Boundary Characterization and Control	6
3.	CORRELATED WACKER SILSO	7
	3.1 Background	7
	3.2 Comparisons of Grain Boundary Electrical Activity	7
4.	HYDROGEN PASSIVATION INFLUENCES ON ELECTRICAL BEHAVIOR	12
	4.1 Background	12
	4.2 Experimental Conditions	13
	4.3 Scanned-Laser Spot Studies	13
5.	PHYSICAL AND CHEMICAL CHARACTERIZATION	21
	5.1 Ellipsometric Characterization	21
	5.2 Auger Spectroscopy	22
	5.2.1 Native Oxides	22
	5.2.2 Thermal Oxides	23
	5.2.3 Hydrogenated Native Oxides	23
	5.2.4 Discussion of Auger Results	28
6.	GRAIN BOUNDARY ACTIVATION	29
7.	LATERAL DLTS MEASUREMENTS	36
8.	MATRIX STUDIES	43
	REFERENCES	53
	ACKNOWLEDGEMENTS	55

INVESTIGATION OF PHOTOVOLTAIC MECHANISMS IN POLYCRYSTALLINE THIN-FILM SOLAR CELLS

T. A. Temofonte, J. R. Szedon and T. W. O'Keeffe
Westinghouse R&D Center
Pittsburgh, Pennsylvania 15235

ABSTRACT

This program treats three tasks. Modelling of polycrystalline silicon solar cells is being done by workers at Penn State who are reporting separately on this and the remaining areas of their responsibility. Westinghouse effort on the second task involves measurement technique development to assess the utility of DLTS methods in characterizing polycrystalline silicon that was deliberately doped with Ti during growth. Difficulties encountered with lateral DLTS measurements are discussed. In this approach, modulation of the grain boundary, double-depletion region produces the entire DLTS signal. Major effort has been applied in the third task area: grain boundary characterization and control. The most significant accomplishments to date have involved laser scanning of slices of Wacker SILSO polysilicon having nearly identical grain structure. By using various kinds of treatments and by comparing treated and untreated substrates having nearly identical grain structure, we have demonstrated control of grain boundary photocurrent suppression (ΔI_{ph}) over the range $1\% \leq \Delta I_{ph} \leq 40\%$.

LIST OF FIGURES

		Page
Figure 1	Twenty-nine slices (5 cm x 5 cm) of Wacker SILSO polycrystalline silicon correlated by grain-pattern comparisons at Westinghouse	8
Figure 2	Reflection images (a) and (b) using 6328 Å laser spot scanning as well as photocurrent images (c) and (d) and single scan photocurrent amplitude traces (e) and (f) of MIS cells in two slices of correlated Wacker SILSO silicon	9
Figure 3	Photocurrent image corresponding to Fig. 2c using 1.15-μm laser spot scan	11
Figure 4	Plasma-tube system used for atomic hydrogen-passivation studies	14
Figure 5	Reflection images produced by scanned 6328 Å laser light spots of MIS cells in (a) control and (b) plasma-hydrogenated Wacker SILSO. Selected grain boundary features are indicated to show structural correlation.	15
Figure 6	Photocurrent images (a) and (b) using 6328 Å laser spot scanning as well as single scan photocurrent amplitude traces (c) and (d) for control and plasma-hydrogenated material, respectively	17
Figure 7	Reflection images (a) and (b) and photocurrent images (c) and (d) taken with a 1.15-μm wavelength laser spot scan for control and hydrogenated material, respectively	19

LIST OF FIGURES (Continued)

		Page
Figure 8	Auger spectra for <100> silicon having native oxide surface	24
Figure 9	Auger spectra for <100> silicon surface having 15 Å thermal oxide	25
Figure 10	Auger spectra of hydrogenated-silicon surface initially and after .5, 3, and 5 min of backsputtering	26
Figure 11	Auger spectra for hydrogenated-silicon surface of Fig. 6 after 10, 15, 20, and 25 min of backsputtering	27
Figure 12	Reflection image (a) photocurrent image (b) and single scan photocurrent amplitude traces taken with a 6328 Å wavelength laser light spot scan of MIS cell fabricated in control (untreated) material	31
Figure 13	Reflection image (a) photocurrent image (b) and single scan photocurrent amplitude trace taken with 6328 Å laser light spot scan of MIS cell in heat-treated material	32
Figure 14	Reflection image (a) photocurrent image (b) and single scan photocurrent amplitude trace taken with 1.15-μm laser light spot scan of MIS cell in control material	34
Figure 15	Reflection image (a) photocurrent image (b) and single scan photocurrent amplitude trace taken with 1.15-μm laser light spot scan of MIS cell in heat-treated Wacker SILSO	35
Figure 16	Montage of photocurrent images obtained using a 40-μm diameter laser (6328 Å) light spot scan of a 1 cm^2 MIS test structure in heat-treated Wacker SILSO silicon	38

LIST OF FIGURES (Continued)

		Page
Figure 17	Photocurrent image (a) and single scan photocurrent amplitude trace for one 0.25 cm x 0.25 cm region of control sample	39
Figure 18	Photocurrent image (a) and single scan photocurrent amplitude trace for one 0.25 cm x 0.25 cm region of heat-treated sample shown in Fig. 16	40
Figure 19	Conventional DLTS spectra of MIS diode in heat-treated Wacker SILSO silicon	42
Figure 20	SEM view of test structure for lateral DLTS measurements mounted on square sapphire substrate	44
Figure 21	Illuminated current-voltage behavior (ln I_{ph} vs. V_{oc}) of six small MIS cells in base-line Ti-CZ polysilicon	47
Figure 22	Illuminated current-voltage behavior (ln I_{ph} vs. V_{oc}) of five small MIS cells in CZ polysilicon doped with 2×10^{13} cm^{-3} Ti	48
Figure 23	Illuminated current-voltage behavior (ln I_{ph} vs. V_{oc}) of MIS cells in CZ polysilicon doped with 1×10^{14} cm^{-3} Ti	50
Figure 24	Illuminated current-voltage behavior (ln I_{ph}^{avg} vs. V_{oc}^{avg}) averaged for a number of MIS cells in base-line, 2×10^{13} cm^{-3}, and 1×10^{14} cm^{-3} Ti-doped material	51

LIST OF TABLES

		Page
Table 1	Process Sequence for MIS Solar Cells Using Aluminum as a Top Barriers Metal	29
Table 2	Status of Matrix Studies	45

1. SUMMARY

The most significant accomplishments to date have involved scanned-laser spot characterizations of grain boundary effects on photocurrent in Wacker SILSO polycrystalline silicon. We have been able to demonstrate control of ΔI_{ph}, peak photocurrent suppression at a boundary, relative to the local average value of photocurrent, over the range $1\% \leq \Delta I_{ph} \leq 40\%$. During the course of this work, we have shown that grain boundaries in polycrystalline silicon exhibit a range of electrical activity, both initially and after various treatments used to control grain boundary properties. Significantly reduced grain boundary electrical activity resulted from atomic hydrogen passivation. Significant increases in ΔI_{ph} at grain boundaries have been produced by high-temperature heat treatment (15 min at 500°C, 2 hr at 900°C, 15 min at 500°C) in N_2.

The foregoing results were obtained with a He-Ne laser operating at 6328 Å wavelength. At this wavelength, the penetration depth in silicon is approximately 2.5 μm. We have also obtained laser-scanned results at 1.15 μm, having a penetration depth of about 300 μm, somewhat greater than the sample thickness of ∿200 μm. Laser-scanned photoresponse images at 1.15 μm of hydrogenated samples indicate that for the plasma conditions used, deep grain boundary passivation was not achieved. However, 1.15 μm scanned-photoresponse images of heat-treated samples indicate strong activation of grain boundaries throughout the bulk of the material.

There are three important aspects of the methodology used in obtaining the foregoing results. (1) The results were obtained using direct photocurrent measurements of solar cells. Thus, they can be correlated directly with solar cell performance. (2) The cell-processing temperatures for MIS barrier formation were much lower than those used for PN junction cells. For example, cell-processing temperatures did not exceed 95°C after plasma hydrogenation. The use of MIS solar cells in

this diagnostic context avoids ambiguities and confusion that generally accompany other, high-temperature barrier fabrication methods.
(3) Comparisons of photocurrent behavior and cell behavior were made before and after the various activation/deactivation treatments using essentially equivalent grain boundaries found in correlated pieces of Wacker SILSO silicon. The ability to make this type of comparison was very useful in the heat treatment studies. It was crucial in the hydrogenation experiments since the maximum value of ΔI_{ph} prior to plasma treatment was $\lesssim$ 15%.

MIS cells fabricated in hydrogenated Wacker SILSO generally had lower open-circuit voltage and poorer fill factor compared to control samples. In the best case, V_{oc} reduction was about 20 mV relative to control cells. We attribute this to surface damage effects produced by the plasma. In cells with a tunneling oxide produced by low-temperature plasma oxidation, open-circuit voltage values were 150-250 mV lower than for controls. Poor fill factor in hydrogenated cells is attributed to a much thicker tunneling insulator than in control cells. Auger sputter profiling of hydrogenated samples revealed a compositionally complex surface layer which is about four times thicker than the oxides in conventional MIS control devices.

With the foundation provided by laser-scanned detection of controlled grain boundary activity in correlated Wacker SILSO silicon, we began efforts dealing with DLTS measurements. MIS solar cells have been fabricated in both untreated (control) and high-temperature treated, correlated Wacker SILSO silicon. These were made using ∿200-μm diameter Aℓ dots. Over these, continuous layers of thin aluminum (80 Å) and SiO_2 (700 Å) were deposited. Treated substrates having activated grain boundaries were prepared in order to insure maximum values of grain boundary photocurrent suppression.

This approach was used to increase the likelihood of detecting both conventional and lateral DLTS response. Laser-scanned photoresponse images of the entire 1-cm^2 area of both the control and treated substrates were used to map grain boundary electrical activity. Quantitative comparisons were made by using single-line scan amplitude traces (A-traces) taken for equivalent grain boundaries. Two main conclusions were drawn from these results. (1) For all the equivalent grain boundaries that we characterized, larger values of ΔI_{ph} were observed for high-temperature treated substrates than for untreated substrates. (2) Untreated substrates exhibited larger maximum values of ΔI_{ph} than previously observed.

After the initial characterization to identify the most active grain boundaries, both the AR coating and thin-barrier aluminum film were removed, leaving an array of MIS dot contacts within individual grains and on grain boundaries. These permitted conventional DLTS measurements to be made in both regions for later comparison with lateral DLTS results. Based on conventional DLTS data for Wacker SILSO polycrystalline, we calculate a concentration in mid-grain regions of approximately 10^{13} cm^{-3} of a species similar in energy to molybdenum. Calculated concentrations for MIS-contacted grain boundaries were about half that for the mid-grain regions. The species giving rise to the conventional DLTS signal measured for Wacker SILSO polysilicon is not likely to be molybdenum, since molybdenum in the quantities detected would result in much more serious degradation of solar cell characteristics than we observe.

Additional processing was done to provide samples for the lateral DLTS measurement. First, the thick aluminum MIS contacts located over grain boundaries of interest were selectively removed leaving only mid-grain MIS contacts. After removal of the back aluminum ohmic contact and 1 to 2 μm of the underlying silicon, the mid-grain MIS contacts were sintered to give ohmic contacts to both sides of selected grain boundaries. Etching was done to delineate

small silicon bicrystal specimens, each having a single grain boundary across its surface.

We did not observe back-to-back diode behavior or voltage-dependent capacitance behavior for any of these specimens. Absence of a detectable grain boundary barrier in these samples could be due to shunting paths in various regions: (1) at the back side of the substrate associated with the original sintered aluminum; (2) at the front surface or along the sample sides due to a native oxide-induced inversion layer; and (3) within the bulk due to a nonuniform barrier throughout the depth of the material. The absence of rectifying grain boundary barriers using the lateral-contacting technique has precluded lateral DLTS characterization.

Matrix experiments involving comparisons of diffused junctions and MIS solar cells in thinned (50 μm and 150 μm) correlated Wacker SILSO and CZ polysilicon with and without deliberate titanium doping are underway. Such a comparison in thin (∿ 50 μm) polysilicon material should provide greater insight into detailed mechanisms than would similar comparisons for thick (∿ 250 to 500 μm) material. We have developed and verified procedures for both high-temperature processing (to 960°C) and for mechanical handling (particularly for photolithography) which minimize substrate breakage. Final sample processing incorporating these refinements is underway to complete the matrix study.

Initial matrix studies have involved characterization of low-temperature MIS cells fabricated in undoped (control) and deliberate Ti-doped (2×10^{13} cm^{-3} and 1×10^{14} cm^{-3}) Czochralski polycrystalline silicon at various fixed levels of illumination. Values of both I_{ph} and V_{oc} monotonically decrease with increasing Ti concentration. Based on these detailed room-temperature characteristics, we infer a consistent increase in the diffusion-current component of diode-opposing current as the titanium concentration increases. Thus, an increase in Ti concentration produces a decrease in minority-carrier lifetime. This is the first confirmation of this effect in cells produced without involving high-temperature diffusion processing.

2. INTRODUCTION

2.1 Contract Objective

Modelling, characterization, and control of grain boundary influences on the performance of cells fabricated in polycrystalline silicon represent the primary objectives of this program. We intend to study the utility of selected measurement techniques for characterizing grain boundary influences on cell performance. In particular, we will investigate the role of a selected impurity (titanium) in Czochralski-grown polycrystalline material.

2.2 Approach

2.2.1 Task 1: Modelling

At Penn State, modelling efforts begun earlier will be extended to arbitrarily shaped grains. A Green's function approach will be used and initially tested by comparison with the Fourier-Bessel series results. Methods for treating an assembly of grains having a distribution of sizes will be explored.

2.2.2 Task 2: Measurement-Techniques Development

At Penn State, refinement of laser-scan apparatus and theoretical interpretation of measurements will be the focus of the effort. Capacitively detected photoresponse, open-circuit photovoltage, and photoconductivity data will be taken on polycrystalline silicon materials, compared, and interpreted. The attributes, disadvantages, and meaning of the data generated by each of these measurements will be determined.

At Westinghouse, the method of Deep-Level Trap Spectroscopy (DLTS) will be examined as a means of quantifying the density of traps associated with deliberate introduction of titanium as an impurity. In

particular, the method of Spencer et al. applied in polycrystalline GaAs[1] will be tried. With this method, ohmic contacts applied to either side of a grain boundary allow using the depletion regions on either side of the grain boundary to sense the DLTS signal. In this way, sensitivity to the grain boundary effects is enhanced by eliminating signals associated with an overlying surface barrier.

2.2.3 Task 3: Grain Boundary Characterization and Control

At Westinghouse, effort on this task will be applied to extend the results obtained on Wacker SILSO material to Ti-doped polycrystalline CZ silicon.

Thin-film polycrystalline silicon material will be simulated either by chemical etching or by ion beam milling of the back surface after formation of the collecting barrier. Chemical etching has been successful in preparing material of ∿50-μm thickness in which cells were found to have reduced values of V_{oc} due to back contact recombination. This simulation, particularly with Ti-doped material, should be valuable in assessing the effectiveness of back-surface field action in potentially low-cost, thin-film polycrystalline cells.

A matrix study of several promising barrier formation, grain boundary passivation, and back-surface, field-region processing methods will be examined. Specifically, ion implantation, solid state and gas source diffusions, and hydrogenation will be considered.

At Penn State, heterojunction cells using M-S, MIS, and homojunction barriers will be explored as required for correlation of device behavior with modelling predictions and with the lateral photosensing techniques.

3. CORRELATED WACKER SILSO

3.1 Background

Throughout this program, we have made use of Wacker SILSO silicon. Careful inspection of the grain structure on the pieces, as received, has permitted us to establish approximately the relative location within the original cast ingot of a number of slices. It was felt that the use of such "correlated" material would allow for more quantitative comparisons of grain boundary behavior before and after various treatments. We refer to specific grain boundaries in such material as being essentially equivalent.

Examples of correlated Wacker SILSO slices are shown in Fig. 1. Based on analysis at Westinghouse, these pieces were considered to be sequentially ordered, i.e., in a larger set of correlated slices. MIS barrier structures have been fabricated by low-temperature methods in such material to permit direct electrical assessment of various grain boundary treatments.

3.2 Comparisons of Grain Boundary Electrical Activity

Fig. 2 shows results of scanned-laser spot characterizations for MIS cells fabricated at the same time on two correlated SILSO slices. In Figs. 2a and 2b, laser reflection images are shown. Careful inspection of these photographs reveals grain features on the two slices which are nearly identical.

In order to establish equivalence in terms of grain boundary electrical activity, it is necessary to measure photocurrent response at and near grain boundaries. We do this by measuring the photocurrent output of cell structures as a function of laser spot location.

Figures 2c and 2d are laser photocurrent response images which include two (indicated) specific grain boundaries common to both slices. The HeNe laser used to produce these images operates at 6328 Å and has a penetration depth in silicon of $\sim$ 2.5 μm. The laser spot size in this instance was about 4 μm.

Figure 1 Twenty-nine slices (5 cm x 5 cm) of Wacker SILSO polycrystalline silicon correlated by grain-pattern comparisons at Westinghouse

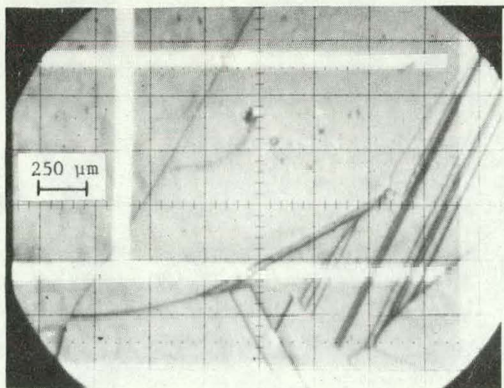

(a)

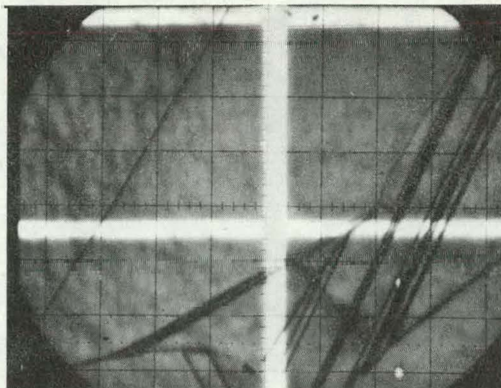

(b)

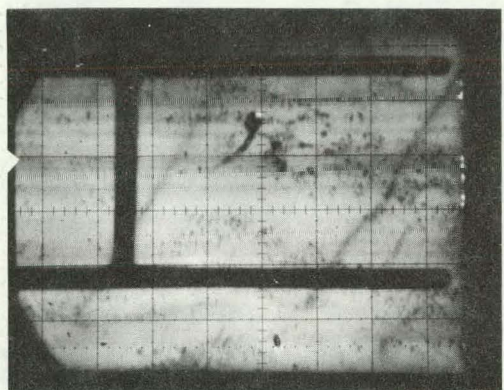

(c)

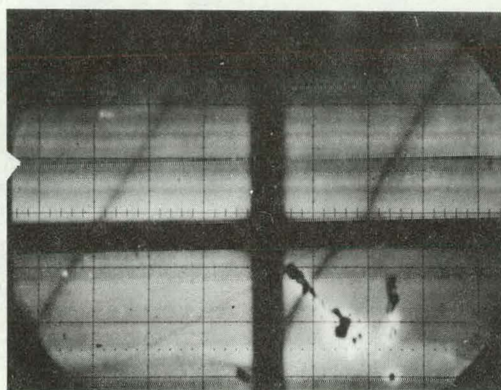

(d)

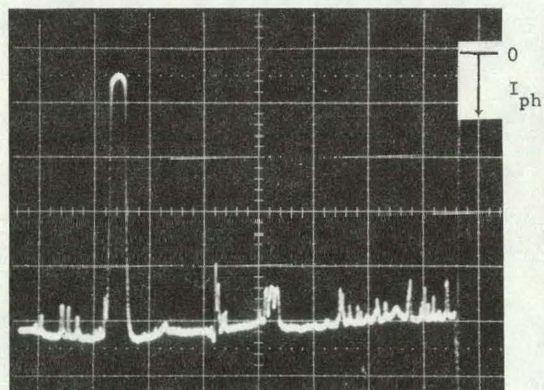

(e)

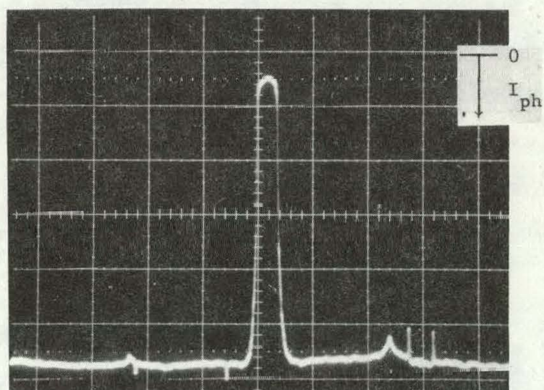

(f)

Figure 2 Reflection images (a) and (b) using 6328 Å laser spot scanning as well as photocurrent images (c) and (d) and single-scan photocurrent amplitude traces (e) and (f) of MIS cells in two slices of correlated Wacker SILSO silicon.

The two lower photographs in Fig. 2 show photoresponse amplitude along a single-scan line (A-traces) taken at approximately equivalent locations on each slice. The cell characterized at the left in Fig. 2 had a somewhat rougher surface than its companion at the right. As a result, the photocurrent A-trace, shown in Fig. 2e, is more complex than for the other cell.

Two cusps in photocurrent response for similar grain boundaries are indicated on each of the A-traces of Figs. 2e and 2f. We define a quantitative measure of photocurrent suppression (ΔI_{ph}) at a grain boundary by the expression

$$\Delta I_{ph}\ (\%) = \frac{\langle I_{ph} \rangle_{loc} - I_{ph}^{min}}{\langle I_{ph} \rangle_{loc}} \times 100$$

Here the local average value of photocurrent ($\langle I_{ph} \rangle_{loc}$) is used in scaling the reduction in photocurrent associated with its minimum value (I_{ph}^{min}) at the grain boundary. For the cells shown in Fig. 2, the values of ΔI_{ph} for each grain boundary in question differed by no more than about 3%. In subsequent experiments, we considered as significant differences in ΔI_{ph} for comparable grain boundaries which exceeded $\sim$3%.

Figure 3 shows the photocurrent image corresponding to Fig. 2c for a 1.15-μm wavelength scan. In this case, the substrate thickness ($\sim$200 μm) and laser penetration depth are approximately the same. The surface roughness effects seen in Fig. 2c are not evident in Fig. 3. However, the two features showing measurable ΔI_{ph} in Fig. 2e are also evident in Fig. 3. We infer from this that both grain boundaries are active throughout the substrate. We also note that there is a relatively more responsive region near the right side of the cell which shows clearly for the deeply penetrating light scan but not for the shallow penetration scan. This could be explained if the region of the substrate in question is characterized by a longer minority-carrier diffusion length than is the adjacent material.

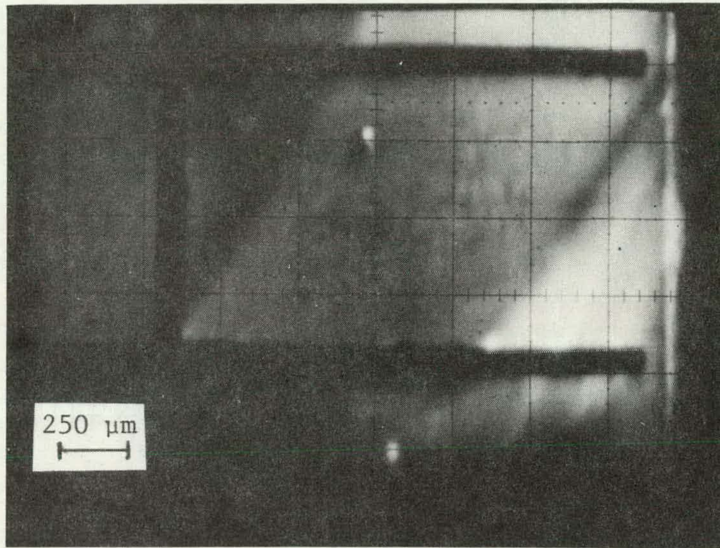

Figure 3 Photocurrent image corresponding to Fig. 2c using 1.15-μm laser spot scan

We have relied on correlated SILSO material to study in a systematic and quantitative manner effects of heat treatments, including hydrogen passivation on grain boundary photoresponse. These are discussed below.

4. HYDROGEN PASSIVATION INFLUENCES ON ELECTRICAL BEHAVIOR

4.1 Background

Plasma hydrogenation and MIS barrier formation are relatively low-temperature processes with potential usefulness in producing low-cost, high-performance cells in polycrystalline silicon. Atomic hydrogen passivation of grain boundaries has previously been demonstrated using several techniques. Some of these involve use of nonbarrier structures[1,2,3] for which some cell-related information has been derived, though indirectly. Other approaches have involved use of high-temperature diffused junction barriers.[4] These offer the advantage of direct measurement of photocurrent suppression or photocurrent enhancement at electrically active grain boundaries. However, measurements using junction barriers are limited by both the influences of high-temperature processing on material properties,[2] and by the possibility that the diffused emitter region causes slow penetration of atomic hydrogen.[4]

We have previously shown[5,6,7] that laser-scanned MIS solar cells in polysilicon provide detailed information on grain boundary photocurrent suppression. We have combined low-temperature MIS cell processing with structurally correlated Wacker polycrystalline silicon wafers to study chemical etch effects and plasma hydrogenation of grain boundaries.[8]

4.2 Experimental Conditions

For the current studies, we used the plasma-tube system shown in Fig. 4. The plasma is generated inductively using a nine-turn winding around a closed quartz tube. Radiative heating was used to produce substrate temperatures from 300°C to 400°C. The tube is connected to a turbomolecular pump and a quadrupole mass analyzer (QMA). Unfortunately, persistent problems with the QMA have precluded analysis of the gas composition during operation.

Plasma pressures ranging from 0.5 torr to 10 torr have been studied. We have observed that the plasma collapses in size for pressures above 5 torr. Net power levels of 15 to 75 watts have been used in this work. Early work was done using a substrate temperature of 300°C for 1 hr at 0.5 torr, with a net power of 75 watts.[8]

4.3 Scanned-Laser Spot Studies

MIS cells were fabricated in Wacker SILSO on material hydrogenated with the plasma method described in Section 4.2. Companion cells on material correlated with regard to surface grain structure were fabricated at the same time without plasma exposure. We refer to these specimens as control wafers or cells. Scanned-laser spot evaluations were made of both types of cells. We believe that this approach permits direct and less ambiguous assessment of grain boundary behavior than do those using nonbarrier structures or high-temperature diffused junctions, which are being undertaken by other workers.

Figure 5 shows reflection images produced by a scanned-laser (6328 Å) spot of MIS cells fabricated in control and hydrogenated wafers of Wacker SILSO. Hydrogenation was done using the plasma conditions described in Section 4.2. In Fig. 5a we have labeled a number of points (A through L) to define certain surface features for reference in comparison to the hydrogenated sample (Fig. 5b) and

Dwg. 7738A35

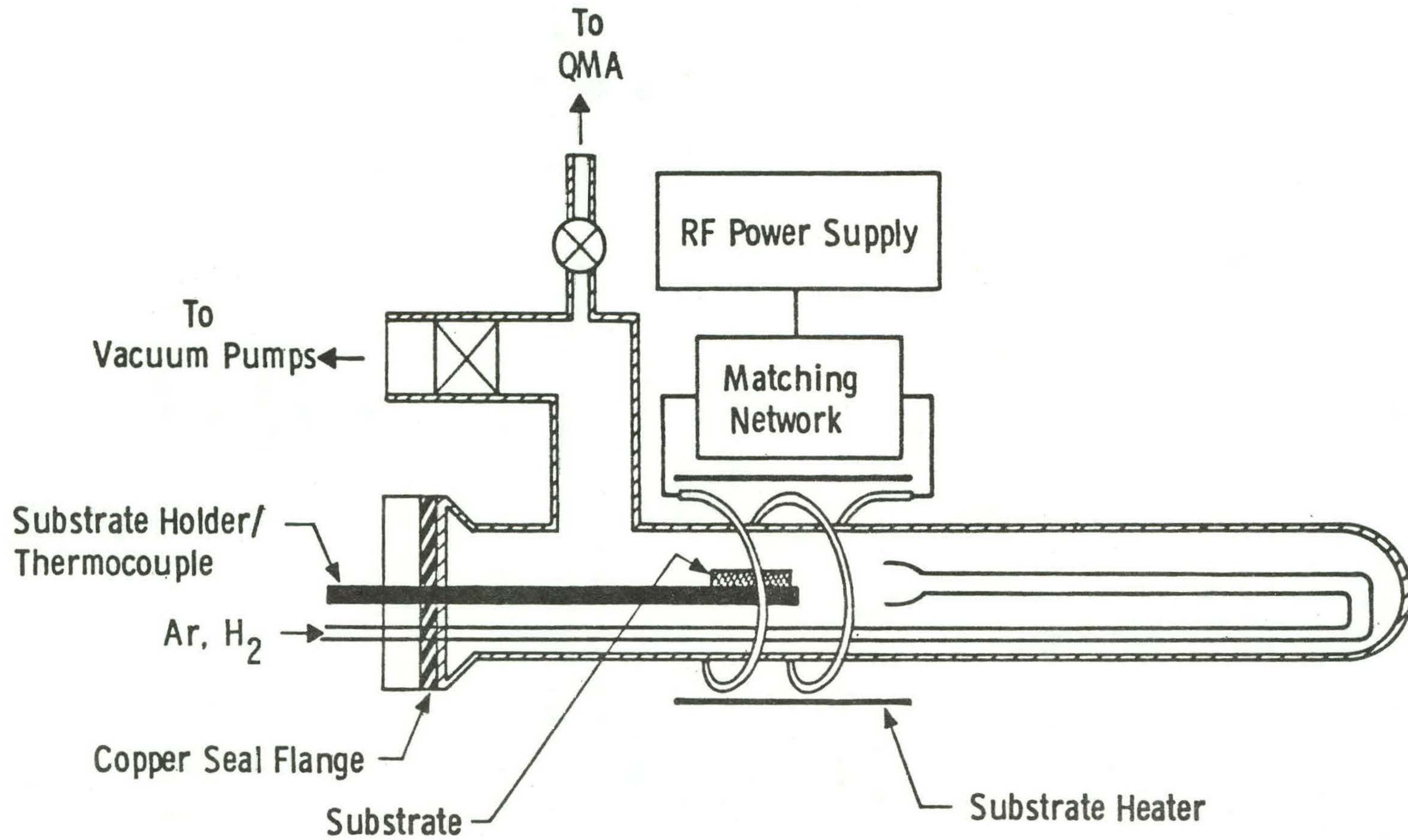

Figure 4 Plasma-tube system used for atomic hydrogen-passivation studies

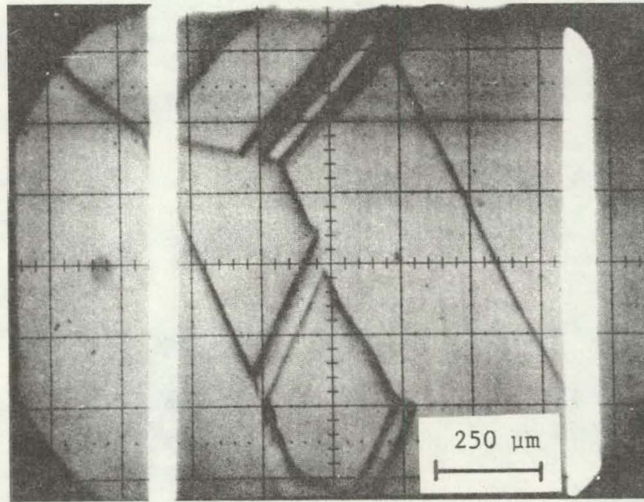

(a)

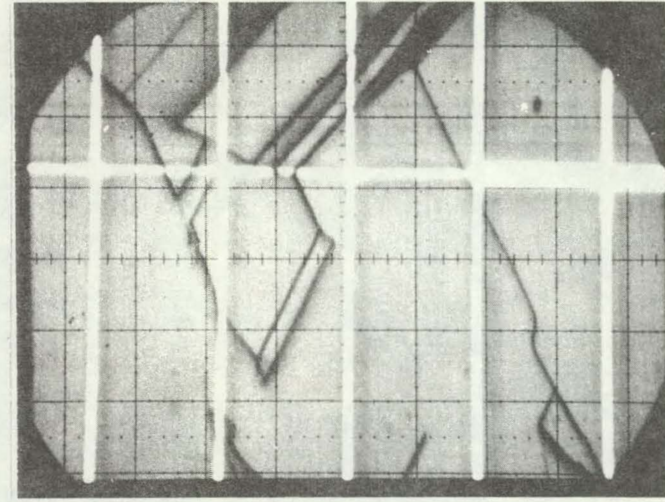

(b)

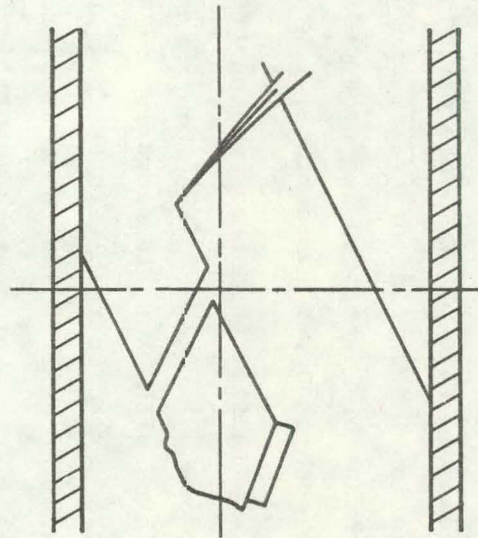

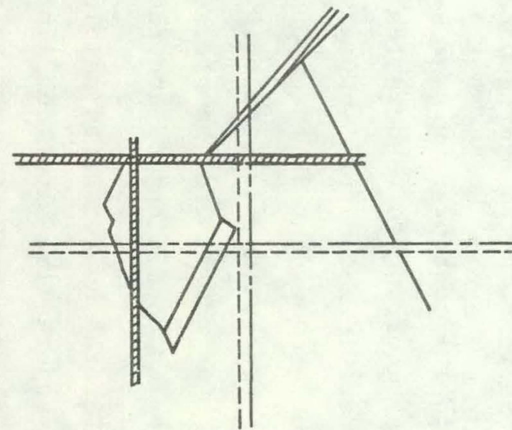

Figure 5 Reflection images produced by scanned 6328 Å laser light spots of MIS cells in (a) control and (b) plasma-hydrogenated Wacker SILSO. Selected grain boundary features are indicated to show structural correlation.

for convenience in discussing features in the photocurrent images of both samples (Figs. 5a and 5b). The surface grain features of both samples are very similar, but note that the area EFGHIJK is shifted up and to the left in the hydrogenated sample.

In the control sample, Fig. 6a shows prominent photocurrent suppression occurring in association with the line features AB, BC, and EF. There is nonuniform suppression along lines CD, DL, and EK, which may not be evident in the reproduced image of Fig. 6a. It was not possible to resolve any structure in the photocurrent image for the path FGHIJK for the control sample, although several images were obtained using different conditions of contrast.

For the hydrogenated sample, the photocurrent image (Fig. 6b) reveals no suppression along the lines A'B, B'E, or E'F. We interpret absence of photocurrent suppression in these regions as evidence for passivation by the hydrogen plasma treatment. We note that the original photographs show slightly enhanced response along BE', which may not be evident in this print. This may also be interpreted as an effect of passivation. Reduction of grain boundary photocurrent loss could permit discernment of light trapping produced by topological features developed by the etch used for the surface.

In Fig. 6b, strong photocurrent suppression occurs along the lines HI and IJ. Three spots of locally strong suppression are associated with, but lie slightly to the left of, the line JKL. These features were discernible in the original reflection-image photographs for the hydrogenated and the control samples. The spots are not visible in the photocurrent images for the control sample (Fig. 6a) against the background of generally low response for the area in question.

Comparisons were made of photocurrent A-traces for comparable regions in both specimens (Figs. 6c and 6d). The value of ΔI_{ph} is about 10% in the vicinity of point c and along the upper part of line AB in the control sample. For the hydrogenated specimen, ΔI_{ph} was 1% less in the corresponding region.

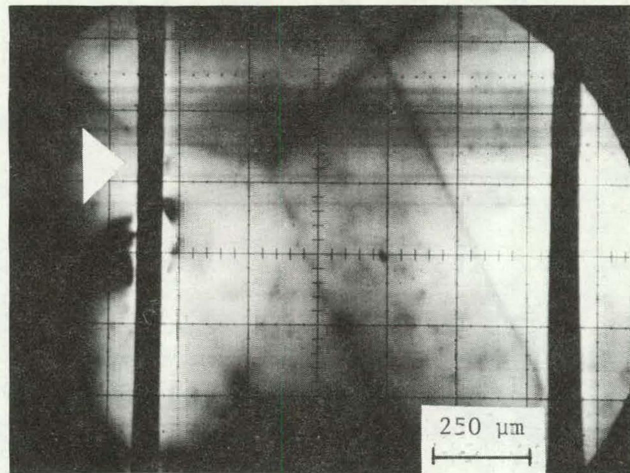

(a)

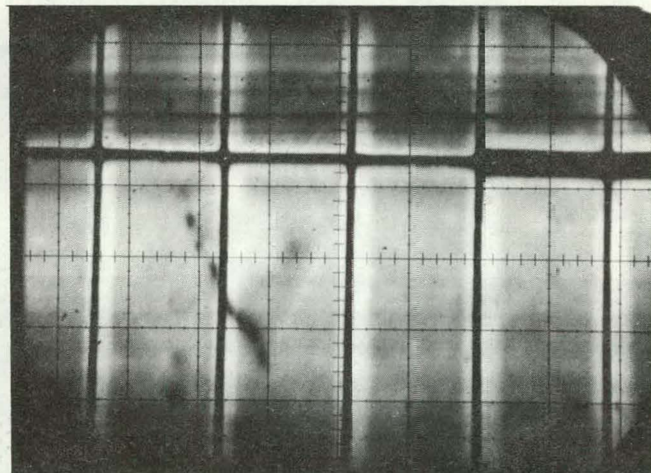

(b)

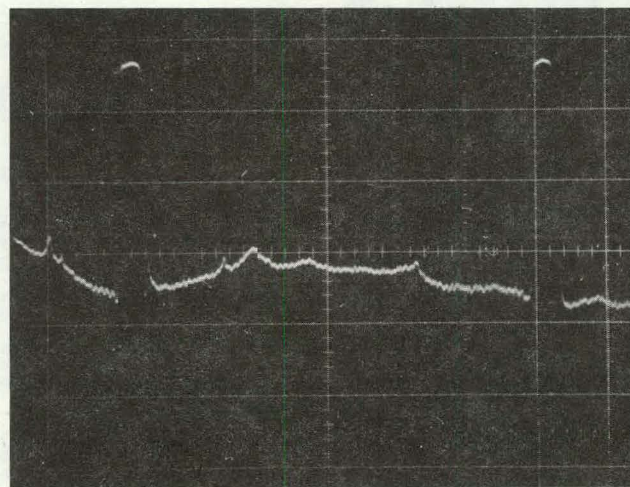

(c)

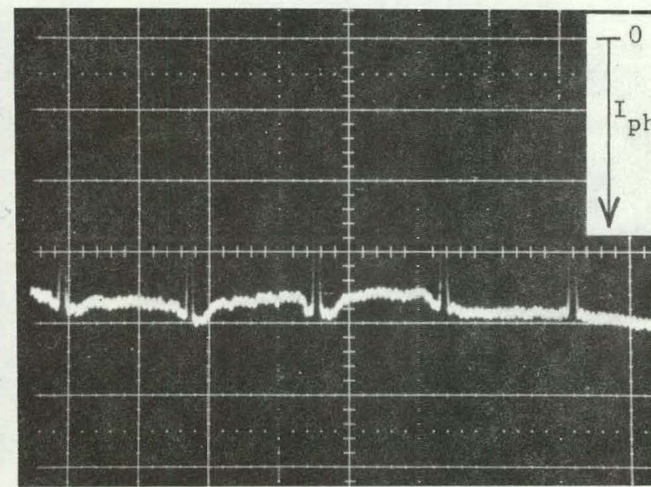

(d)

Figure 6 Photocurrent images (a) and (b) using 6328 Å laser spot scanning as well as single scan photocurrent amplitude traces (c) and (d) for control and plasma-hydrogenated material, respectively.

These investigations with a 6328 Å laser spot show hydrogen plasma passivation of simple grain boundaries which intersect the surface in long straight lines. Since light of this wavelength has a shallow (2.5 μm) penetration depth in silicon, information on the activity of grain boundaries at greater depths requires the use of longer wavelength light. Use of a tunable dye laser would be an ideal method to permit multispectral scanning with a wide range of penetration depths. We are presently limited to using a He:Ne laser at 1.15-μm wavelength with light of about 300 μm penetration depth for these studies.

In Fig. 7, results of scanning with a 1.15-μm wavelength laser spot are shown for areas of interest on the samples discussed above. These photographs are the first results we obtained using the alternate laser sources. One of the features of these images is the presence of interference fringes in the reflection and (with a complementary sense) in the photocurrent modes. We do not understand why these do not appear in the 1.15-μm scan of Fig. 3. Nonetheless, in the present case, we attribute these to reflection from the back surface of the specimens and to the variations in sample thickness produced by the etch method that was used for surface preparation. Ghost images of the top-surface grain boundaries, such as those of line AB in Fig. 5a, appear displaced to the right in Fig. 7a. These probably indicate grain boundary walls within the wafer that are inclined slightly ($\sim 25^{o}$) away from the normal to the surface. The boundary tilting and the presence of the interference fringes degrade the quality of the photocurrent images and reduce their usefulness for this study.

With the 1.15-μm laser spot, the discernible details of photocurrent suppression in the control specimen (Fig. 7c) are significantly different from those for the shorter-wavelength examination, appearing in Fig. 6a. No photocurrent suppression is detected along the line AB. Line BC is likewise absent in Fig. 7c. Line CD and the upper part of line EF appear, though not sharply. The curving boundary along HIJKL is defined by strong photocurrent. By comparison, for short-wavelength scanning,

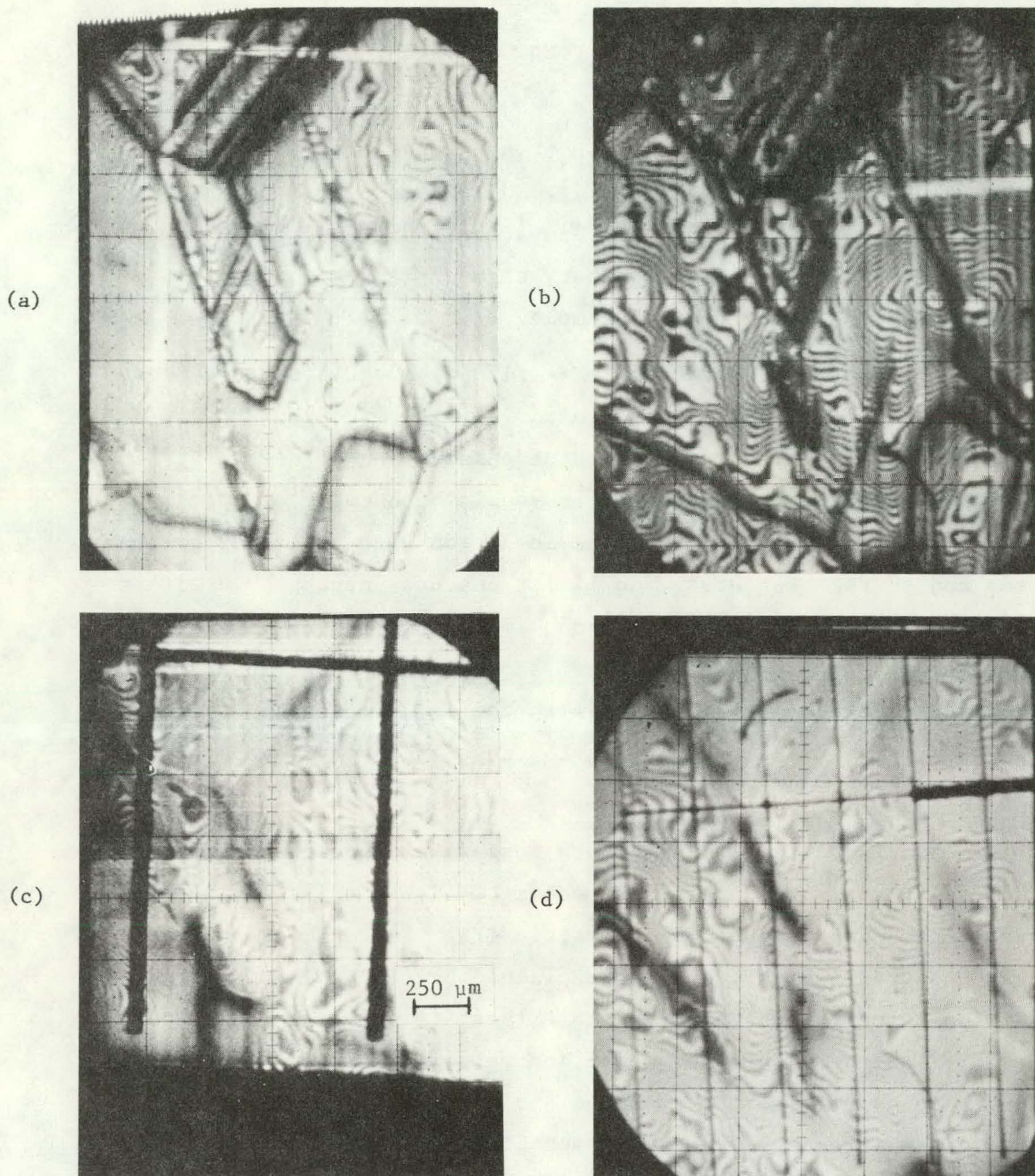

Figure 7 Reflection images (a) and (b) and photocurrent images (c) and (d) taken with a 1.15 μm wavelength laser spot scan for control and hydrogenated material, respectively.

this region exhibited generally lower response, devoid of detail (Fig. 6a).

For the hydrogenated sample, strong photocurrent suppression also occurs along the boundary HIJK (Fig. 7d). Because of the apparent spatial translation of the grain area E'FGHIJK with respect to the other grains, there is no boundary segment corresponding to the straight line DE in the control sample.

Use of deeply penetrating (λ = 1.15 µm) light spot to compare and control hydrogenated Wacker SILSO material with MIS barriers has not elucidated details of the depth of passivation effects at grain boundaries. Strong photocurrent suppression in both types of specimens occurred for long-wavelength light in association with nonlinear grain boundaries and surface features. No linear features appeared in either the long- or short-wavelength photocurrent images for the hydrogenated specimen. For the control specimen, two short sections of linear boundaries appear electrically active with the 1.15-µm scan, but there are no physical features corresponding to these in the hydrogenated specimen.

We had expected to see in both long-wavelength photocurrent images something corresponding to the straight-line details in the short-wavelength scan of the control sample (Fig. 6a). Their absence, even in the control sample, could be explained by (1) grain boundary recombination velocity, which is variable (specifically, decreasing) with depth; (2) high-surface recombination velocity at the intersection of the grain boundary with the specimen surface; or (3) an effective reduction in the interaction of the laser beam and the grain boundary due to the tilt of the latter. Additional study is needed to clarify these issues, experimentally, by using intermediate wavelengths for scanning and theoretically, on predicting photocurrent recombination by inclined grain boundaries.

The current results provide direct evidence (using photovoltaic cell response) for atomic hydrogen passivation of grain boundaries in which possible ambiguities due to subsequent or prior high-temperature heat treatments have been minimized. Other workers[9] have demonstrated hydrogen passivation in polysilicon using the drag probe technique on nonbarrier structures. We suggest that the relevance of such indirect techniques has not been clearly demonstrated. The same workers have demonstrated grain boundary hydrogen passivation in Honeywell SOC polysilicon. This work, done in cooperation with D. Zook, involved LBIC scans of diffused-SOC polysilicon diodes. These results provide more direct evidence for passivation but unfortunately are clouded by the possibility of changes in grain boundary properties that can occur during high-temperature (e.g., diffusion temperatures) heat treatments. This phenomena is discussed in Section 7. Hydrogen passivation has also been demonstrated in diffused epitaxial solar cell structures.[10] Again, these results are clouded by uncertainties associated with high-temperature treatment effects. For this case, a short 1/2 hr, 500°C vacuum anneal results in poorer solar cell characteristics than before hydrogenation.

Our MIS solar cells fabricated in plasma-hydrogenated Wacker SILSO polysilicon exhibit poorer fill factors compared to control samples. Ellipsometric measurements of hydrogenated single-crystal substrates have indicated the presence of much thicker surface oxides than one would expect. A thick surface oxide ($\geq$ 20 Å) would provide a large contribution to the tunneling impedance of this device and would produce fill-factor degradation.

5. PHYSICAL AND CHEMICAL CHARACTERIZATION

5.1 Ellipsometric Characterization

We have experienced some difficulty in reproducing oxide thickness values (as indicated ellipsometrically) on polysilicon surfaces after plasma hydrogenation. As vacuum leaks were eliminated

in a step-by-step manner, the indicated oxide thickness increased in a step-by-step fashion, contrary to expectation. In subsequent plasma experiments involving an oxygen-containing ambient, we have observed that increasing the oxygen flow rate (relative to the argon and hydrogen flow rates) at constant total-system pressure (500 microns) results in a monotonic reduction in film thickness just after hydrogenation.

Preliminary evidence indicates that a thinner oxide results when the sample is heat treated in a hydrogen atmosphere immediately outside the plasma region, as opposed to within the plasma region. Definitive assessment of such effects will require further study. Cell measurements on hydrogenated polysilicon having ellipsometrically indicated oxide thicknesses of $\gtrsim$19 Å have shown consistent full-factor degradation. This is what one would expect for tunneling-limited resistance effects for oxide thicknesses in this range.

5.2 Auger Spectroscopy

MIS solar cells fabricated using plasma-hydrogenated silicon surfaces have characteristically shown varying degrees of fill-factor degradation. We have explored the possibility that plasma hydrogenation results in thicker oxides than expected, thus introducing tunneling resistance to the devices. Auger sputter profiling was used to compare hydrogenated silicon surfaces with thin (∿ 15 Å) thermal oxides and with surfaces having native oxides (∿ 9 Å thick). Results for these three types of specimens are shown in Figs. 8 through 11.

5.2.1 Native Oxides

The native oxide specimen was produced by etching the single-crystal silicon sample for 1 min in concentrated HF followed by rinsing for 15 min in flowing ultra-pure water. This specimen was then loaded into the Auger vacuum system with less than 15 min ambient exposure.

Figure 8 gives Auger spectra of the native oxide initially and after 1 min of in-situ sputtering. Three energies are marked by arrows in Fig. 8. These are associated with three chemical states of silicon: unbonded silicon at $\sim$92 eV,[11] bonded silicon in SiO_2 at 75 $\pm$ 1 eV,[11] and bonded silicon in SiO_x ($x < 2$) at approximately 80 eV.[12,13] The spectrum for the surface of the native oxide specimen in Fig. 8 shows all three peaks, with a large value for the ratio of the free-to-bonded peak amplitudes. The oxide peaks are suppressed after a short (1 min), in-situ backsputtering. Other samples receiving identical chemical surface treatment have been measured ellipsometrically. These initially have indicated oxide thicknesses of $\sim$9 $\pm$ 2 Å.

5.2.2 Thermal Oxides

Still other single-crystal samples with identical chemical surface treatment have been deliberately oxidized at 500°C in O_2. Ellipsometrically indicated thicknesses for these are 14 $\pm$ 1 Å. Auger spectra for such a sample are shown in Fig. 9. For the surface, the free silicon peak is smaller than the oxidized silicon peaks. Also, the oxidized silicon peaks are still present after 4 min of in-situ backsputtering. Since the nature of ellipsometric measurements for such thin films of SiO_x results in an over-estimation of film thickness, it is clear that small differences in film structure and thickness are at least qualitatively detectable using Auger techniques.

5.2.3 Hydrogenated Native Oxides

We have also used Auger methods to study native oxide surfaces that have been exposed to atomic hydrogen for 45 min at 300°C in an inductively generated plasma. Total system pressure was maintained at 0.5 torr. The carrier gas for these experiments was argon, and some oxygen was unintentionally present. The Auger spectra for such a sample are shown in Figs. 10 and 11. The surface spectrum for the sample is similar to that for the oxidized sample shown in Fig. 9. Multiple peaks

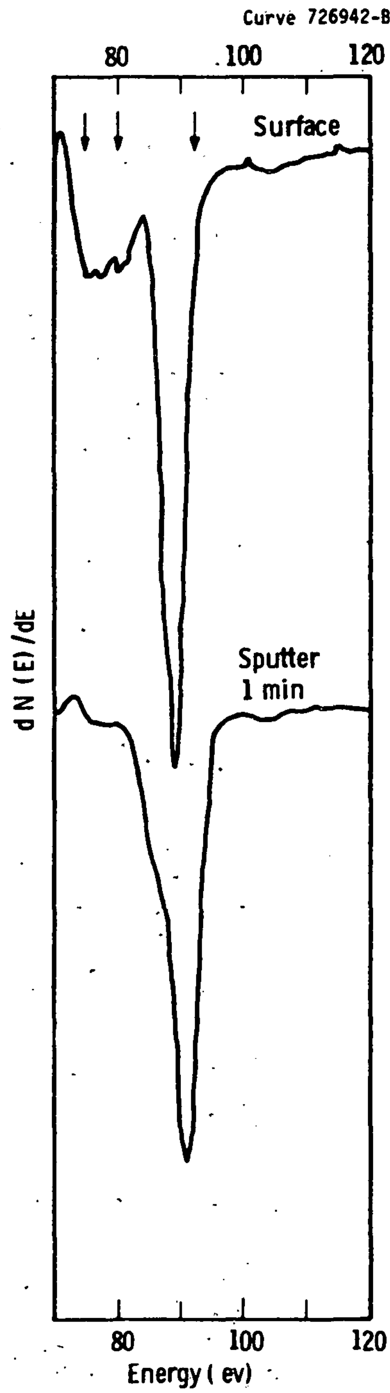

Figure 8 Auger spectra for <100> silicon having native oxide surface

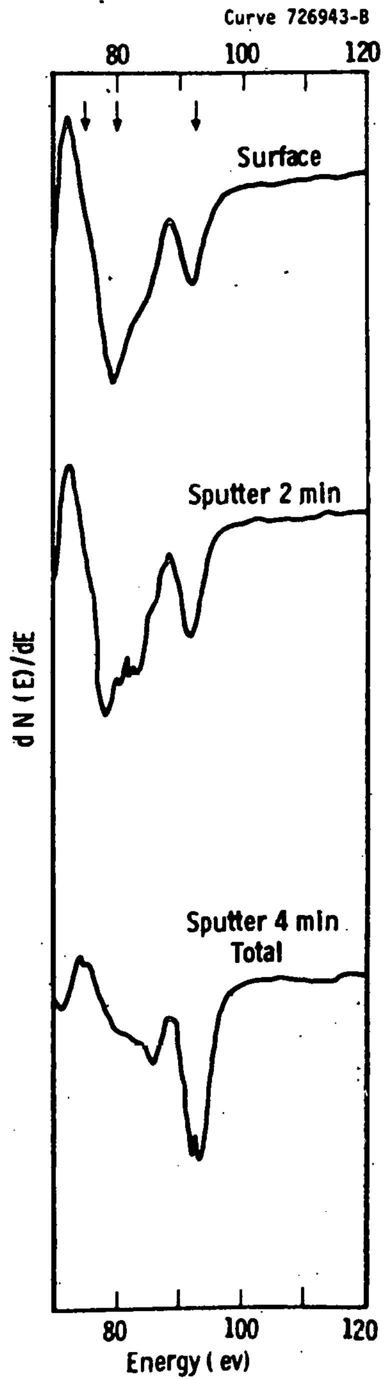

Figure 9 Auger spectra for <100> silicon surface having 15 Å thermal oxide

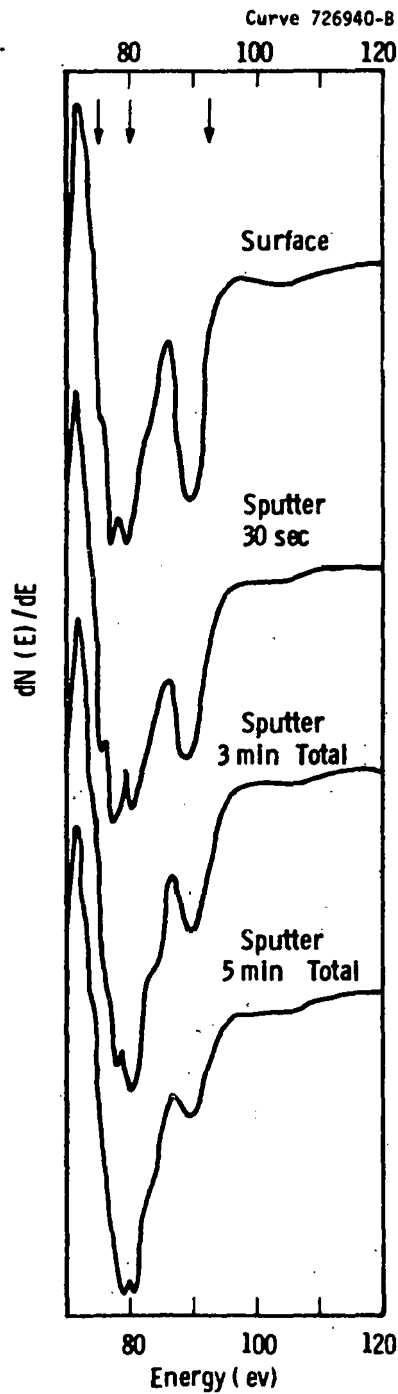

Figure 10 Auger spectra of hydrogenated-silicon surface initially and after .5, 3, and 5 min of backsputtering

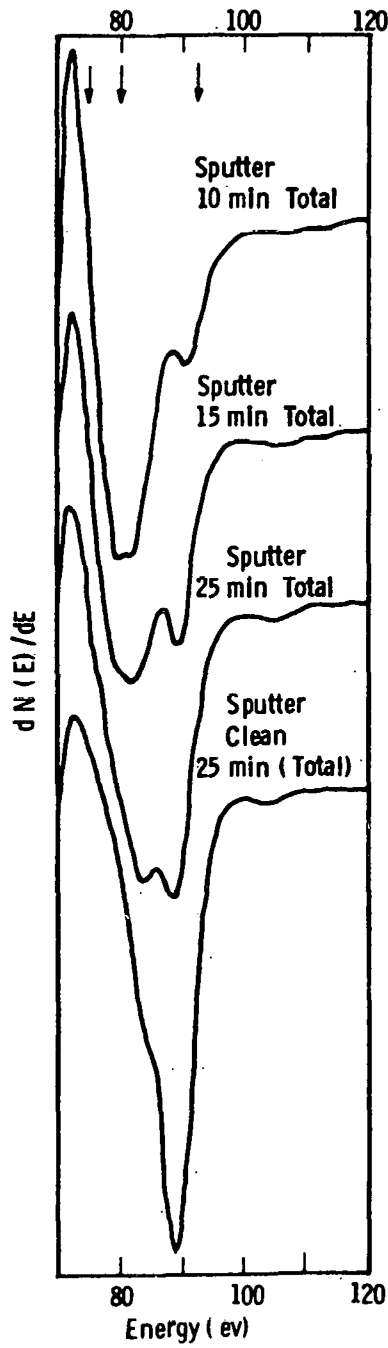

Figure 11 Auger spectra for hydrogenated-silicon surface of Fig. 6 after 10, 15, 20, and 25 min of backsputtering

occur for silicon bonded to oxygen, which may be indicative of various silicon-oxygen bonding states, e.g., SiO_2, SiO, etc. Note that as the surface is gradually backsputtered, in-situ, the ratio of free silicon to bonded silicon decreases significantly. Note also that after about 10 min of sputter-etching, this ratio begins to increase. Finally, after 25 min, the bonded-silicon peak cannot be resolved from the free-silicon peak. The peak near 80 eV, which is present after atomic hydrogenation, has previously been reported to be reduced to zero by annealing in molecular hydrogen.[14]

5.2.4 Discussion of Auger Results

A number of compositions may exist in the thin "surface-oxide" region individually or collectively for plasma-hydrogenated silicon specimens. These may include SiO_2, SiO, SiH, and α-Si. The presence of such a layer might affect PN junction performance by influencing surface recombination or by introducing grid metallization contact-resistance effects. Such a layer would be expected to affect MIS and inversion layer cells in particular.

We have seen series resistance problems with MIS cells fabricated in hydrogenated Wacker SILSO silicon. In these cases, ellipsometric measurements -- which were interpreted without considering the ambiguity of surface composition just mentioned -- have indicated oxide thickness values of 25 to 45 Å. By adjusting the argon, hydrogen, and oxygen composition, we have produced films with indicated thicknesses as low as 19 Å. Series resistance effects for cell structures in this latter case are reduced over the previous case. While we have demonstrated MIS cells in hydrogenated polysilicon in which there is significant grain boundary passivation, there are some potential problems in controlling surface layers. These problems will require consideration if solar cells -- even those using PN junctions -- are to be fabricated by methods which extract the maximum benefit from atomic hydrogenation passivation of grain boundaries.

6. GRAIN BOUNDARY ACTIVATION

Redfield has shown that high-temperature treatments (900 to 1000°C) in a nitrogen atmosphere produce detectable surface electric fields at grain boundaries in Wacker SILSO material.[15] A liquid-crystal film was used to indicate the presence of the electric field.

In the present work, we have made MIS barrier solar cells in correlated pieces of Wacker SILSO material. This approach has permitted a direct, unambiguous assessment of heat-treatment effects on grain boundary photocurrent suppression. Since the MIS barrier formation step is done at temperatures of 500°C or less, this approach avoids the drawbacks of cells with PN junctions produced by high-temperature diffusion. An outline of the processing steps used for fabricating the control cells for these experiments is given in Table 1.

TABLE 1

PROCESS SEQUENCE FOR MIS SOLAR CELLS USING ALUMINUM AS A TOP BARRIERS METAL

1. Clean*/silicon etch/clean;
2. evaporate aluminum back contact;
3. grow oxide and sinter aluminum (500°C/15 min);
4. evaporate aluminum grid;
5. evaporate semitransparent aluminum barrier layer;
6. evaporate AR coating.

The experimental cells were cleaned and then processed with the control cells for steps 2 through 6 in Table 1. Prior to that processing, they were subjected to heat treatment in nitrogen (500°C for 15 min, 900°C for 2 hr, and 500°C for 15 min+) and given an HF etch and rinse.

*See Ref. 8 for cleaning details.

+These temperatures and times are similar to those used for phosphorus diffusions to form shallow NP junctions.

The major effect of the high-temperature heat treatment can be appreciated by comparing the results of He-Ne (6328 Å wavelength) laser spot evaluations shown in Fig. 12 (control sample) and Fig. 13 (heat-treated sample).

Figure 12a is a reflection image of the control-sample surface. Figure 12b is a laser-scanned photoresponse image of the same region. As can be seen, very few grain boundaries (deduced from surface features in Fig. 12a) are electrically active. For those which are electrically active, maximum values of photocurrent suppression are $\leq$ 15%. Figure 12c shows the photoresponse amplitude (A-trace) for a single-line scan depicting this. This behavior is typical of the majority of grain boundaries we have studied to date using laser-scanned MIS barriers.

Figure 13 shows the corresponding behavior for a correlated slice of Wacker polycrystalline silicon that was heat treated _prior_ to MIS cell fabrication. The laser-reflection image of Fig. 13a permits comparison of the degree of similarity of specific grain features from one correlated slice to the next. Figure 13b graphically demonstrates the striking increase in grain boundary photocurrent suppression induced by the high-temperature heat treatment. The darkest grain boundary features in this view correspond to values for ΔI_{ph} of about 40% as estimated from the A-trace shown in Fig. 13c.

Redfield has recently reported work using heat-treated, structurally uncorrelated polycrystalline silicon in which heterojunction barriers using tin oxide were fabricated.[16] Significant grain boundary activation was detected. The heat-treated cells suffered from fill-factor degradation in comparison with control cells.[17] We have not observed this in heat-treated material with MIS barriers.

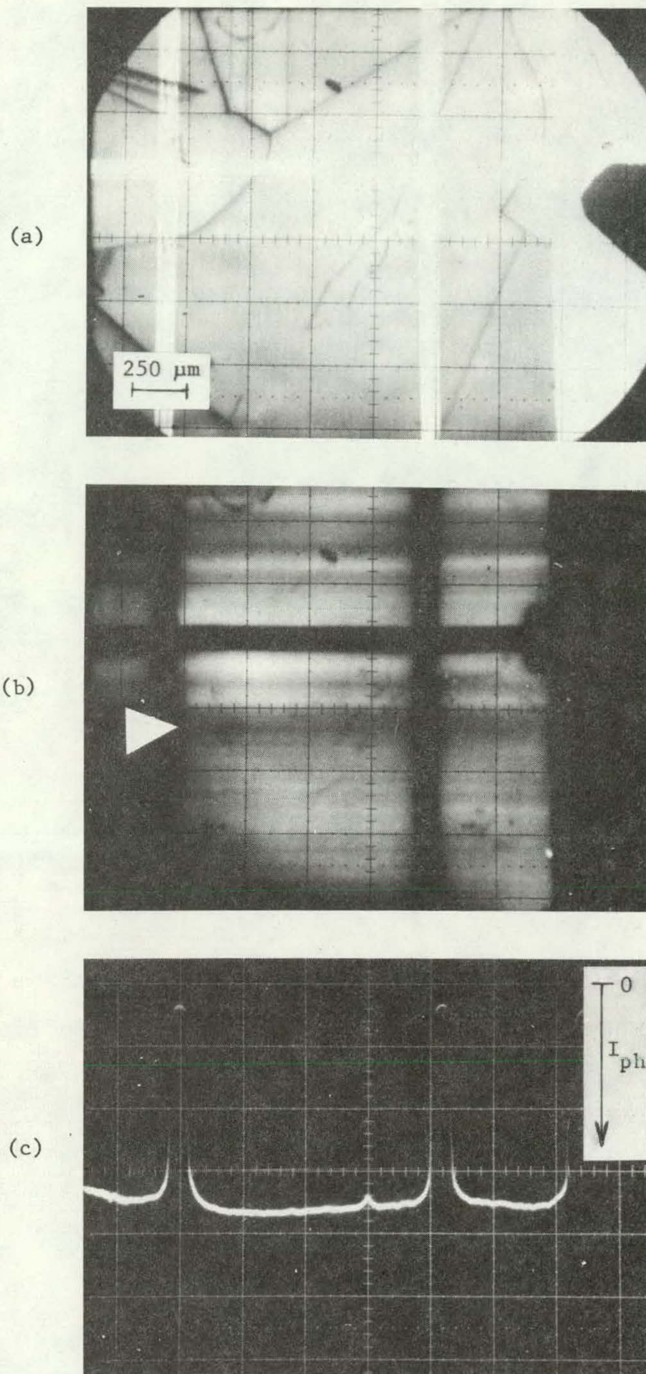

Figure 12 Reflection image (a) photocurrent image (b) and single scan photocurrent amplitude traces taken with a 6328 Å wavelength laser light spot scan of MIS cell fabricated in control (untreated) material.

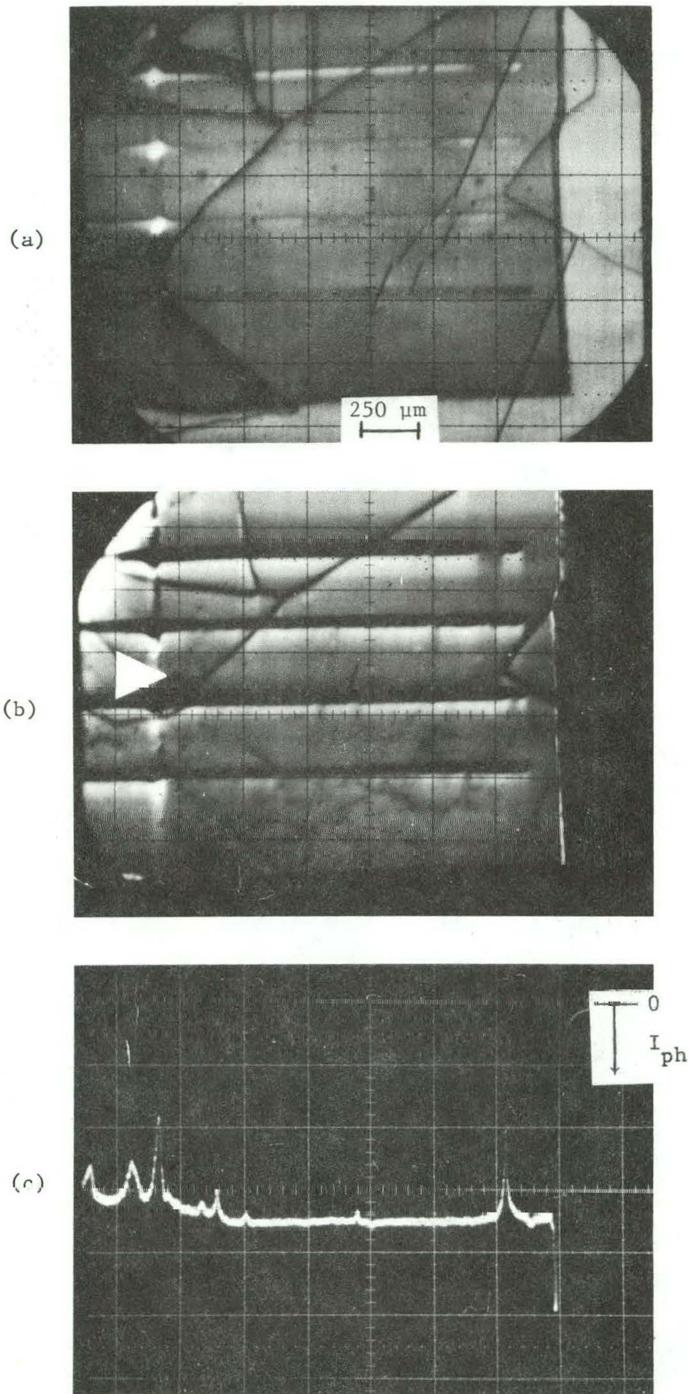

Figure 13 Reflection image (a) photocurrent image (b) and single scan photocurrent amplitude trace taken with 6328 Å laser light spot scan of MIS cell in heat-treated material.

In addition to the laser scan studies with light of shallow penetration, we used a 1.15-μm wavelength laser to characterize cells on heat-treated material. The 300-μm penetration depth of such a light spot is somewhat greater than the 200-μm thickness of the silicon substrate material. Figure 14 gives results for the control material. These are similar to the results of Fig. 11 but with improved image quality. The single-line scan amplitude trace (Fig. 14c) of photocurrent response illustrates the difficulty of assessing values of grain boundary photocurrent suppression in the presence of the interference fringes. Of particular interest is the enhanced response near the center of Fig. 14b, which is associated with an irregular grain boundary in Fig. 14a. For the 6328 Å scan (Fig. 12b), there was only slight photocurrent suppression associated with this feature.

Figure 15 shows the corresponding behavior for the heat-treated Wacker SILSO material. Nearly all of the activated grain boundaries revealed by the 6328 Å wavelength examination in Fig. 13b are evident in the photocurrent image of Fig. 15b for the 1.15-μm wavelength light. This indicates that the activation associated with the high-temperature heat treatment affects grain boundaries throughout the thickness of the wafers. The region corresponding to enhanced photocurrent response in the control sample of Fig. 14b is also evident to the right and slightly below the center of Fig. 15b. Although there appears to be less enhancement for this region in the heat-treated sample, we cannot be more specific about its characteristics.

These results provide direct, unambiguous evidence of the influence of high-temperature heat treatment on grain boundary electrical activity. We do not presently have a model for this behavior. The choice between whether impurity or defect-related mechanisms control grain boundary behavior is currently unclear. Further study will be required to clarify this issue.

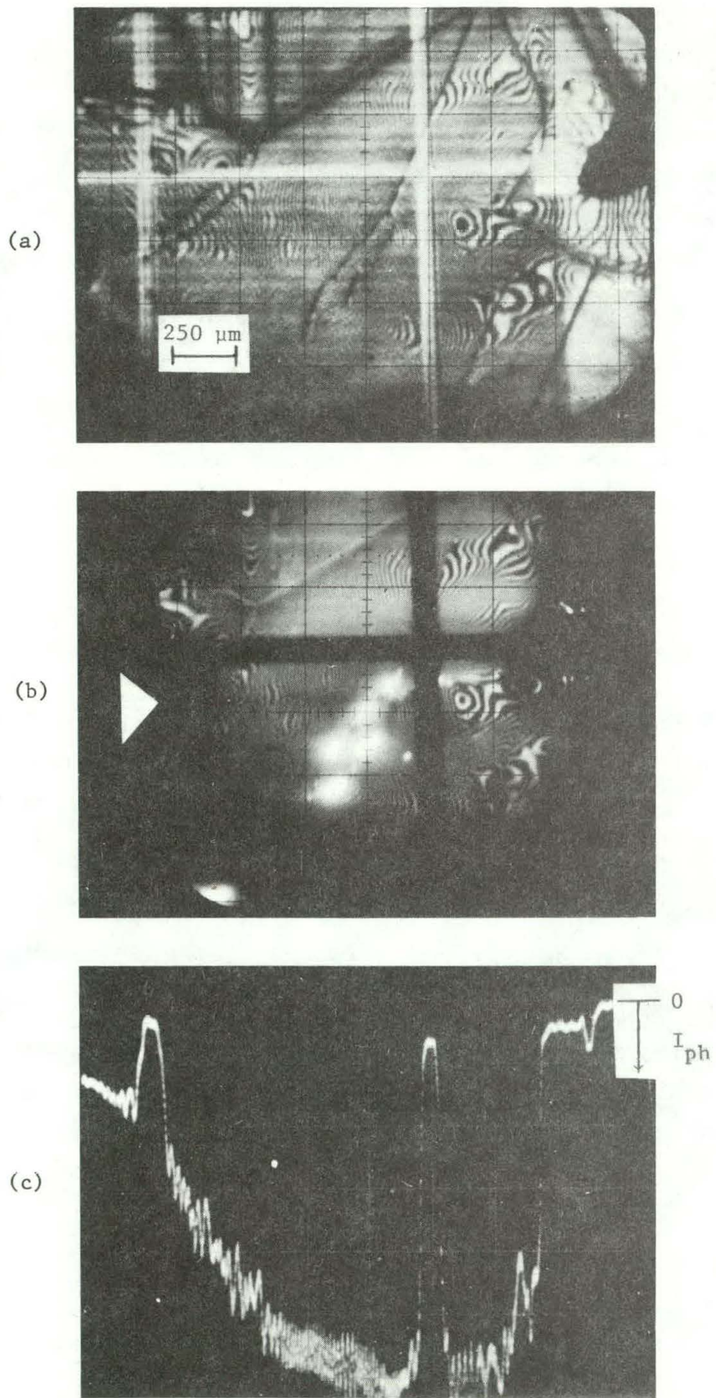

Figure 14 Reflection image (a) photocurrent image (b) and single scan photocurrent amplitude trace taken with 1.15-μm laser light spot scan of MIS cell in control material.

RM-94467

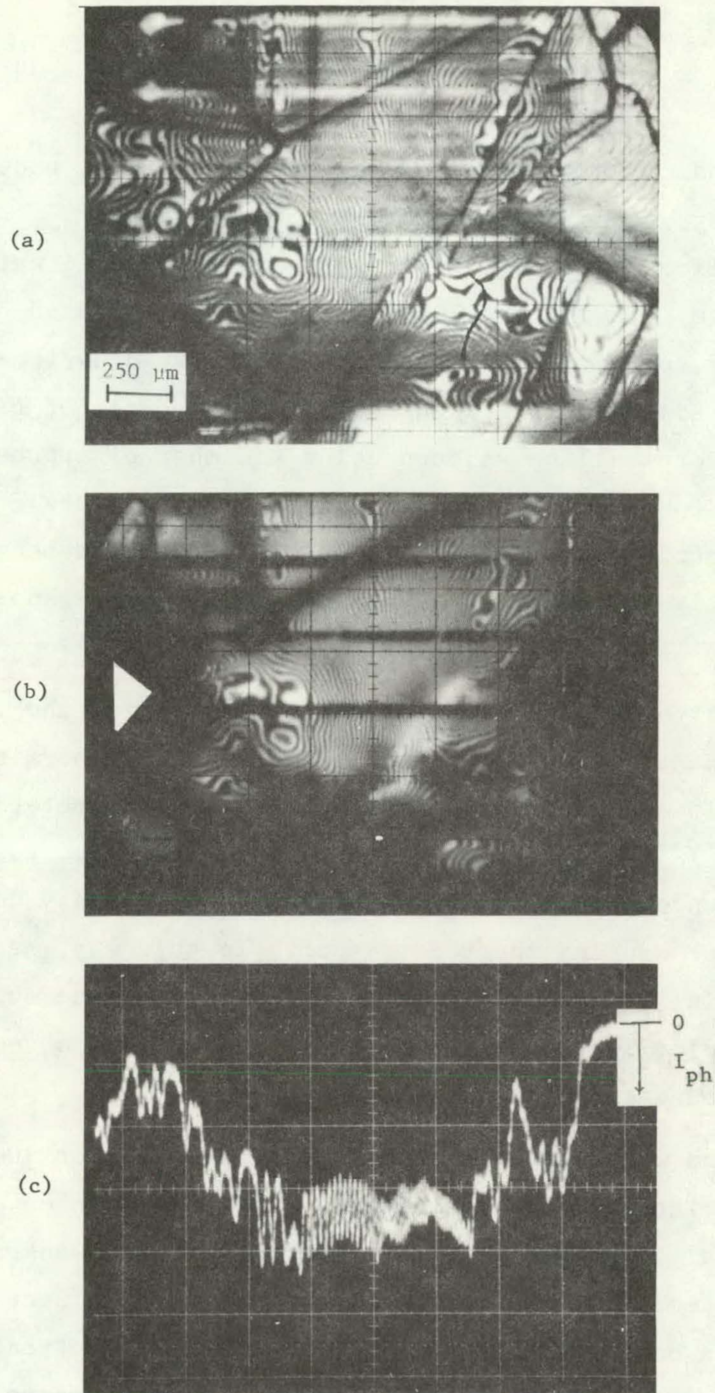

Figure 15 Reflection image (a) photocurrent image (b) and single scan photocurrent amplitude trace taken with 1.15-μm laser light spot scan of MIS cell in heat-treated Wacker SILSO.

7. LATERAL DLTS MEASUREMENTS

Understanding the role of electronically active, undesirable impurities which may be encountered in low-cost, thin-film polycrystalline silicon is an essential part of the overall national photovoltaic program. In the present study, we have focussed on one particular impurity, viz., titanium, which is a known minority-carrier lifetime killer in silicon. We planned to study the role of titanium in Czochralski polycrystalline silicon using a number of approaches. One of these involves comparisons of conventional and lateral[18] Deep Level Transient Spectroscopy (DLTS) data taken on undoped controls, and lightly ($\sim 10^{13}$ cm^{-3}) and heavily ($\sim 10^{14}$ cm^{-3}) doped Czochralski silicon.

Initial efforts have concentrated on perfecting the lateral DLTS approach in Wacker SILSO polycrystalline silicon to permit a smooth transition in applying this technique to Ti-doped material. With the lateral DLTS technique, ohmic contacts are applied to either side of a grain boundary to permit use of the grain boundary double-depletion region for sensing the DLTS signal. In this way, sensitivity to grain boundary influences is enhanced by eliminating the overlying barrier. That barrier introduces parasitic signals which obscure that due to the grain boundary.

Background work was done to establish a basis for judging whether meaningful lateral DLTS measurements could be made on polysilicon material of interest to us. We chose to use Wacker SILSO material. Some material was heat-treated as described in Section 7 to insure strong grain boundary recombination, while other untreated material was carried along as a control. The latter was correlated with the former to allow comparisons with similar grain structures.

The activated grain boundary approach was used to increase the likelihood of detecting lateral DLTS response. MIS solar cells having 1 cm^2 total area were fabricated in both control and treated Wacker SILSO silicon. These were fabricated using thick dots (of about 200-μm diameter) over which continuous layers of thin Al (80 Å) and SiO_2 (700 Å) were deposited.

Scanned-laser (6328 Å wavelength) photoresponse images of the entire 1 cm^2 area of both the control and treated substrates were used to map grain boundary electrical activity in terms of photocurrent suppression. Figure 16 is a montage of photocurrent images obtained with a 40-μm diameter laser spot for the MIS test structure fabricated on heat-treated Wacker SILSO. Note that there are many electrically active grain boundaries evident in this photograph, as expected. Both the control and heat-treated samples were sliced into pieces 0.25 cm by 0.25 cm in size to facilitate both higher resolution (∿4-μm beam diameter) detailed scanning and subsequent mounting onto 4-pin TO-5 headers for DLTS measurements.

Figure 17a is a laser-scanned photoresponse image for one 0.25 cm x 0.25 cm region of the control sample. A photoresponse amplitude line scan (indicated by the white arrow) is shown in Fig. 17b. Values of ΔI_{ph} as high as 31% are deduced for the most active grain boundaries. This is the largest value of ΔI_{ph} that we have ever observed for untreated Wacker SILSO polycrystalline silicon. Previously, the largest values of ΔI_{ph} we had measured were $\leq$ 15%. It is possible that the grain boundaries in Wacker SILSO are more variable than we originally anticipated. It is also possible that some grain boundaries are activated at a much lower temperature -- in this case, by the 500°C processing for the MIS barrier -- than others.

A laser-scanned photoresponse image for the correlated, heat-treated companion sample is shown in Fig. 18a. The corresponding photoresponse amplitude line scan (indicated by the white arrow) is shown in Fig. 18b. The grain boundary region with the highest value of

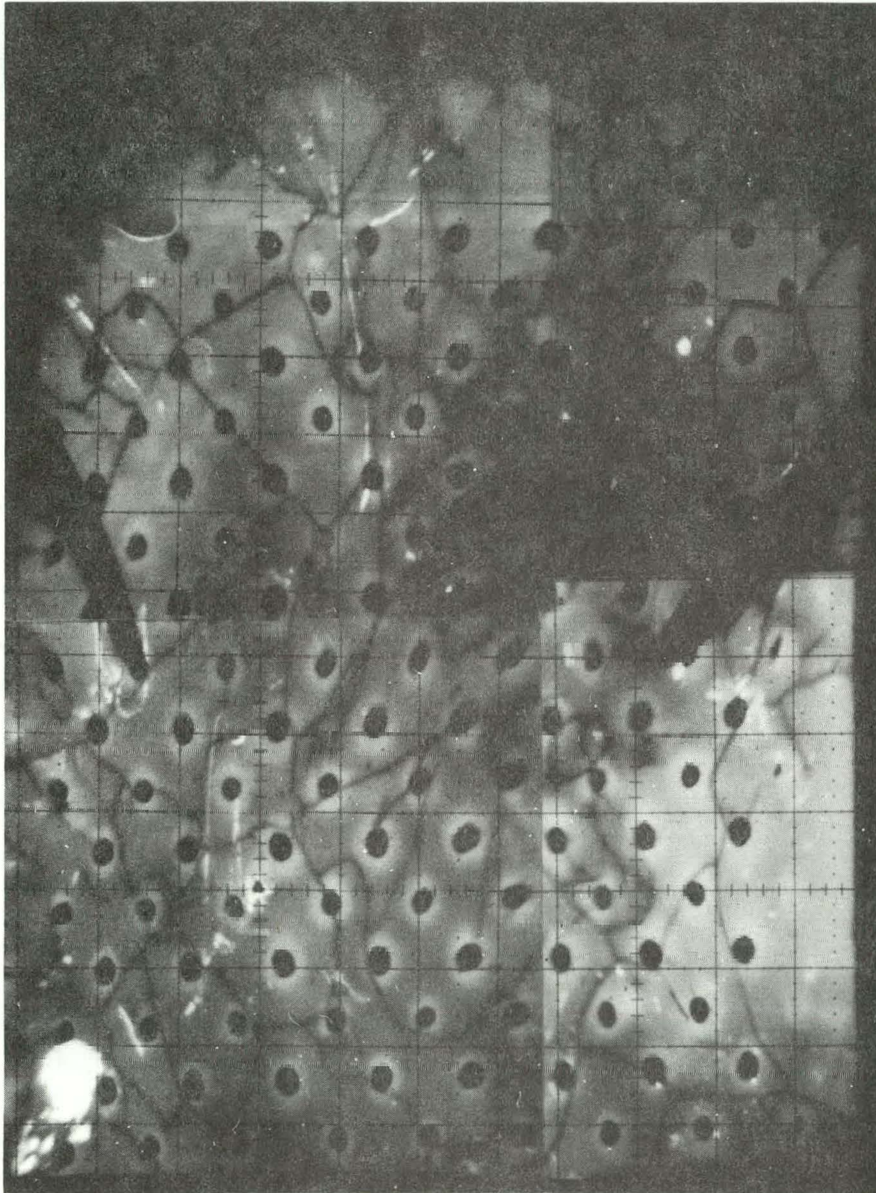

Figure 16 Montage of photocurrent images obtained using a 40-μm diameter laser (6328 Å) light spot scan of a 1-cm^2 MIS test structure in heat-treated Wacker SILSO silicon.

(a)

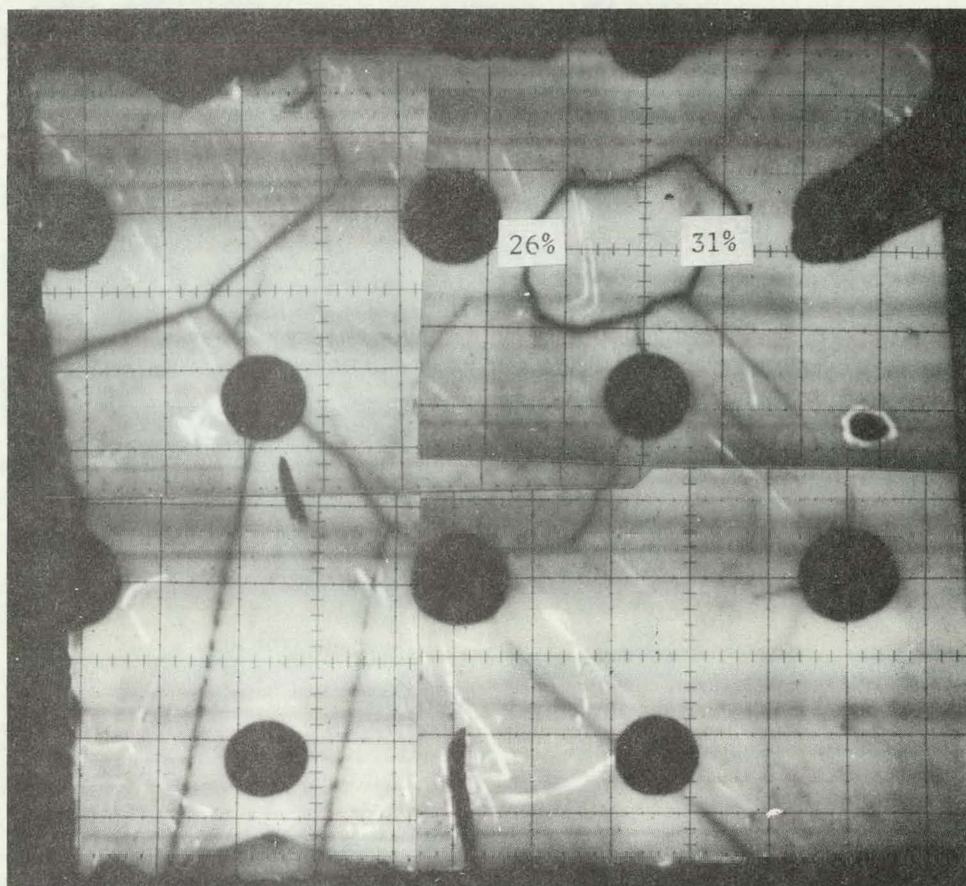

(b)

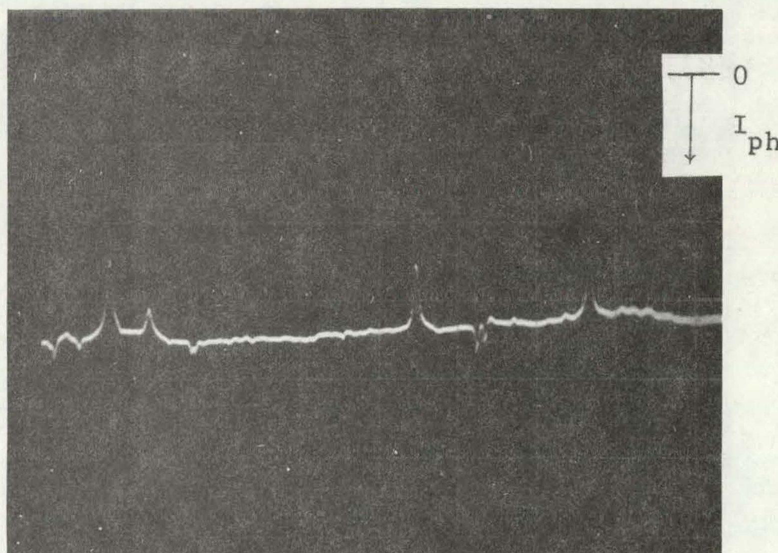

Figure 17 Photocurrent image (a) and single scan photocurrent amplitude trace for one 0.25 x 0.25 cm region of control sample.

(a)

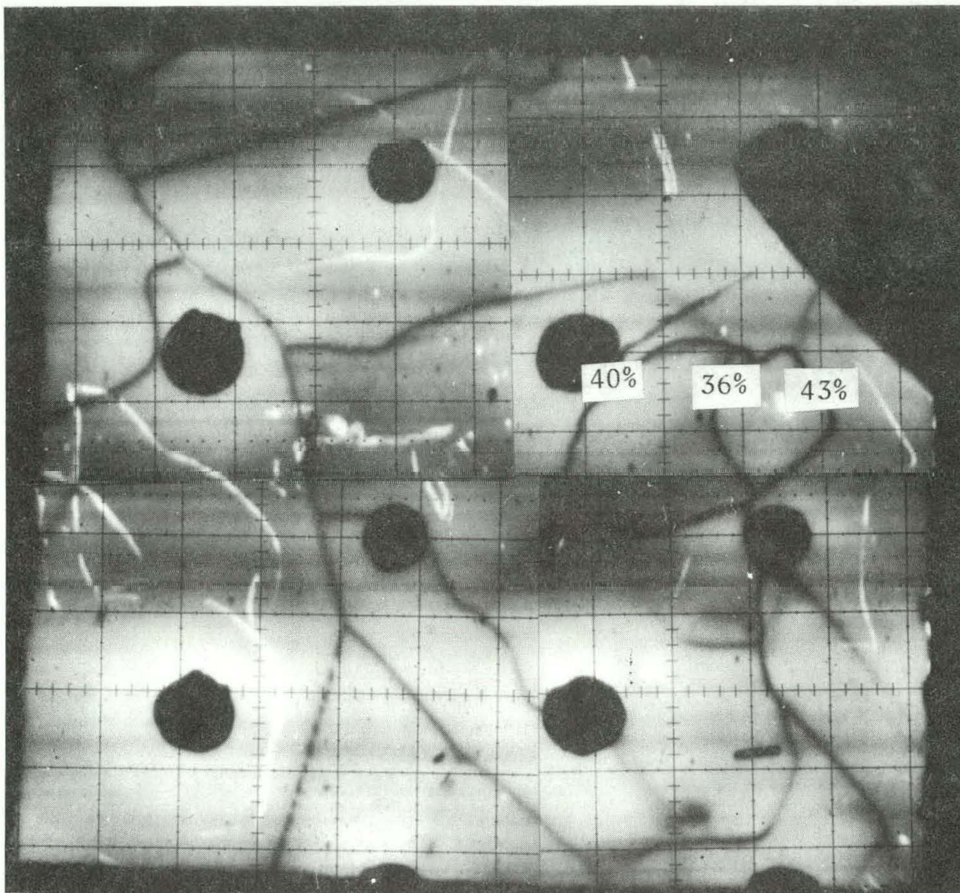

(b)

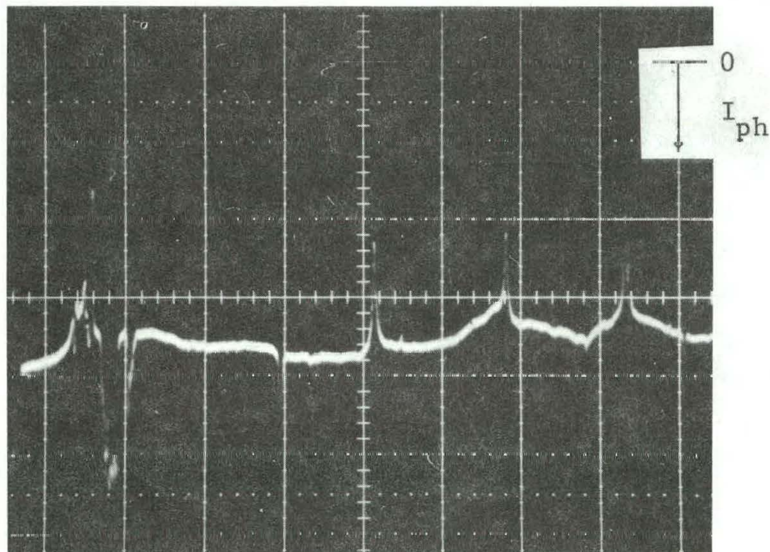

Figure 18 Photocurrent image (a) and single scan photocurrent amplitude trace for one 0.25 x 0.25 cm region of heat-treated sample show in Figure 16.

ΔI_{ph} in the control ($\sim$31%) also had the highest value in the treated sample ($\sim$43%). A number of these 0.25 cm by 0.25 cm die were studied in this way. Values of ΔI_{ph} varied from 11 to 31% for controls and from 16 to 43% for treated specimens. Increases in ΔI_{ph} from control to treated samples for nearly identical grain boundaries ranged from 7% (e.g., 10% to 17%) to 12% (e.g., 31% to 43%).

The preceding approach was used to insure availability of grain boundaries in Wacker SILSO having maximum values of ΔI_{ph}. Such grain boundaries were selectively isolated from the rest by chemically etching out small die, thus producing the desired bicrystal specimens for lateral DLTS experiments. With these specimens, care was taken to remove all of the AR coating, the thin Al layers, any thick Al dots over grain boundaries, and the entire back Al contact (including 1 to 2 μm of underlying silicon). The remaining thick MIS contacts to mid-grain regions were sintered to provide ohmic contacts to these regions. For conventional DLTS measurements, samples were prepared more simply by removing the AR coating and thin aluminum layers, leaving an array of MIS dot contacts within individual grains and on grain boundaries. These permitted conventional DLTS measurements to be made both on mid-grain regions and over grain boundaries for later comparison with lateral DLTS measurements.

Results of conventional DLTS measurements are shown in Fig. 19. We calculate a concentration in mid-grain regions of approximately 10^{13} cm^{-3} of a species similar in energy to molybdenum. Concentrations for MIS contacts overlying grain boundaries were about half that for the mid-grain regions. We believe that impurities in the vicinity of grain boundaries segregate at grain boundaries during the casting and cooling of Wacker SILSO. Impurities that have segregated at grain boundaries appear, from a DLTS point of view, to be electrically inactive. It is unlikely that the species giving rise to the DLTS signal measured for Wacker SILSO polysilicon is molybdenum in concentrations of 10^{13} cm^{-3}, since such a quantity should produce much more serious degradation of solar cell characteristics[19] than we observe.

Curve 731703-A

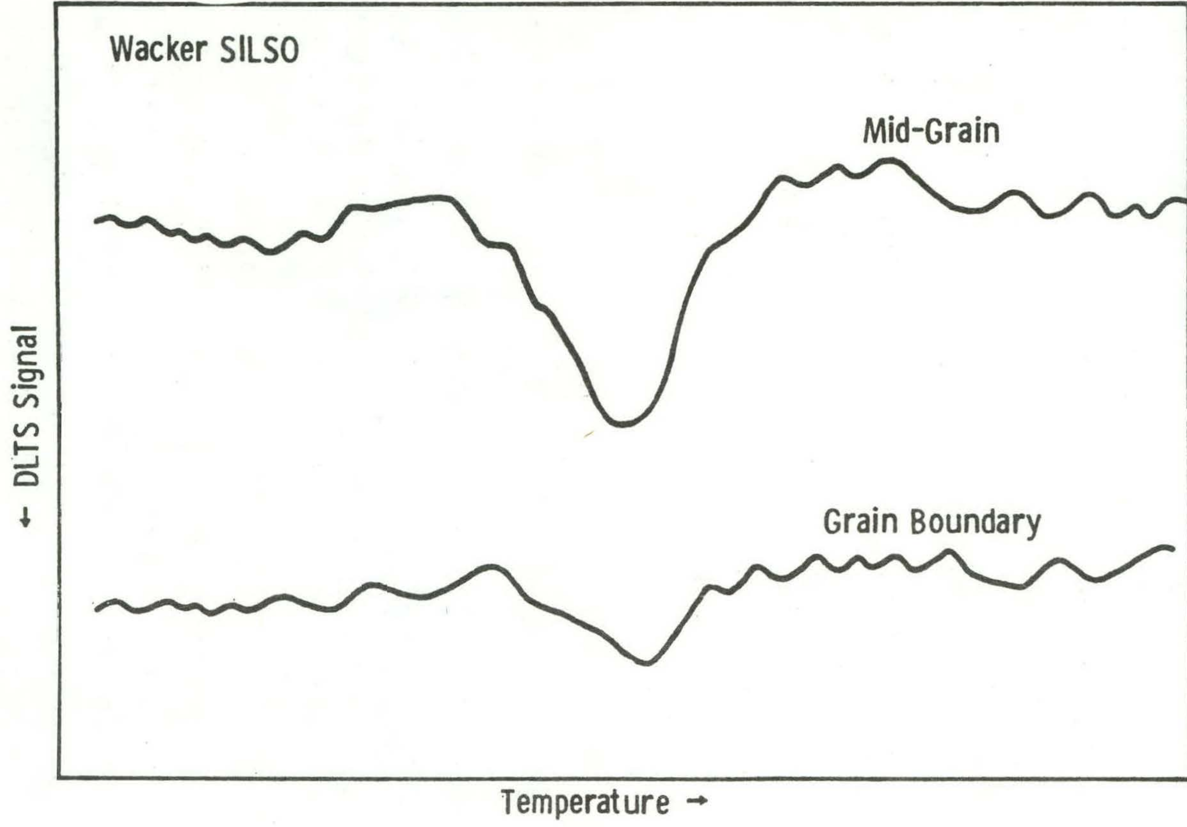

Figure 19 Conventional DLTS spectra of MIS diode in heat-treated Wacker SILSO silicon

Lateral DLTS samples were prepared by isolating grain boundaries in Wacker SILSO having the largest ΔI_{ph}. A typical example of such a test structure is shown in Fig. 20. Conductive epoxy was used to mount gold wires to the MIS contact pads, and the bicrystal itself was mounted to the header with dielectric epoxy. Despite such careful preparation, we did not observe back-to-back rectifying IV behavior or voltage dependent capacitance behavior for any of these specimens. Absence of a detectable grain boundary barrier in these samples could be due to shunting paths in various regions: (1) at the back side of the substrate associated with the original sintered aluminum; (2) at the front surface or along the sample sides due to a native oxide-induced inversion layer; and (3) within the bulk due to a nonuniform barrier throughout the depth of the material. The absence of rectifying grain boundary barriers using the lateral-contacting technique precluded lateral DLTS characterization.

8. MATRIX STUDIES

These studies were begun to examine several promising methods of barrier formation, grain boundary passivation, and back-surface field-region processing. We planned to compare PN junction and MIS barriers in Wacker SILSO polysilicon as well as control and Ti-doped Czochralski polycrystalline silicon.

Table 2 summarizes the various matrix studies planned. Thin-film polycrystalline silicon material has been simulated by chemical etching. We have prepared Wacker SILSO of $\sim$ 50-μm thickness in which MIS cells had reduced values of V_{oc} due to back-contact recombination. This thinning approach, particularly with Ti-doped material, should be valuable in assessing the effectiveness of back-surface field action in potentially low-cost, thin-film polycrystalline cells.

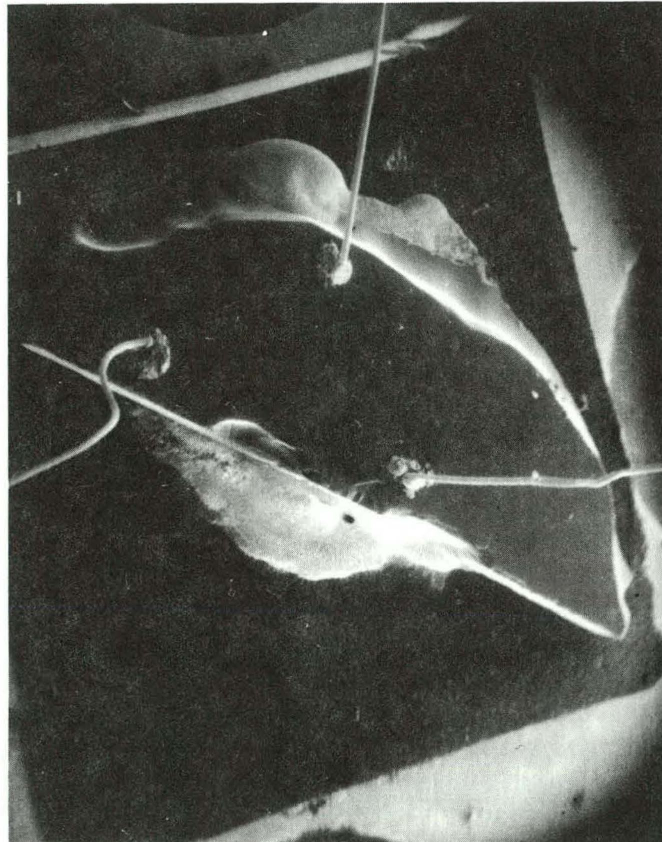

Figure 20 SEM view of test structure for lateral DLTS measurements mounted on square sapphire substrate; gold wires are 1-mil diameter.

TABLE 2

STATUS OF MATRIX STUDIES

	Wacker Thin	Wacker Thick	CZ (undoped) Thin	CZ (undoped) Thick	CZ, (Ti) $\underset{\sim}{\sim}2\times10^{13}cm^{-3}$ Thick	CZ, (Ti) $\underset{\sim}{\sim}1\times10^{14}cm^{-3}$ Thin	CZ, (Ti) $\underset{\sim}{\sim}1\times10^{14}cm^{-3}$ Thick
PN-Junction							
Ohmic	X	X	X	X		X	X
BSF							
MIS							
Ohmic-Standard	X	X	X	X	X	X	X
Ohmic-H Plasma		X		X			X
Ohmic-Heat Treated		X		X			X
BSF-Standard	X	X	X	X		X	X

Some elements of the matrix experiments have already been carried out, e.g., plasma hydrogenation (Section 4) and heat treatment (Section 7) of thick (200 μm) Wacker SILSO having an ohmic back contact and a subsequent MIS-contacted front surface. Standard MIS controls have also been studied in thin (∿ 50 μm) and thick (150-200 μm) Wacker SILSO polycrystalline silicon.

Our initial matrix experiments in control and Ti-doped Czochralski polycrystalline silicon have involved standard MIS barrier processing in base-line (undoped) and deliberately doped (∿ 2×10^{13} cm^{-3} and ∿1×10^{14} cm^{-3}) material. Effects of a strong lifetime killing impurity, such as Ti, are well known from earlier diffused PN junction studies at Westinghouse.[19] In the present case, we expect additionally to obtain information on possible influences of high-temperature processing, by comparing PN junction and MIS barrier cells.

Figure 21 shows the photovoltaic response (ln I_{ph} vs. V_{oc}) of six small MIS cells fabricated on base-line Czochralski polycrystalline silicon. Illumination levels ranging from 0.5 suns to 3 suns were used for these characterizations. Diode ideality factors (n) for these characteristics are near unity with the largest value being 1.2 and the average value being approximately 1.1. Open-circuit voltage values for these diagnostic cell structures were low, due in part to relatively high grid shading. Larger cells having lower grid shading were also fabricated in this base-line material. These had AMI values of $V_{oc} \geq 530$ mV.

Current voltage behavior of Czochralski polycrystalline silicon substrates doped with Ti to approximately 2×10^{13} cm^{-3} is shown in Fig. 22. From a mechanism point of view, these curves are similar to those of Fig. 21. Diode ideality factors are near unity with the maximum value being approximately 1.3 and the average value being about 1.1. However, at a fixed level of illumination, values of both I_{ph} and V_{oc} are lower than in base-line material -- precisely what one would expect for deliberate doping with a lifetime killing impurity such as Ti.

Curve 731704-A

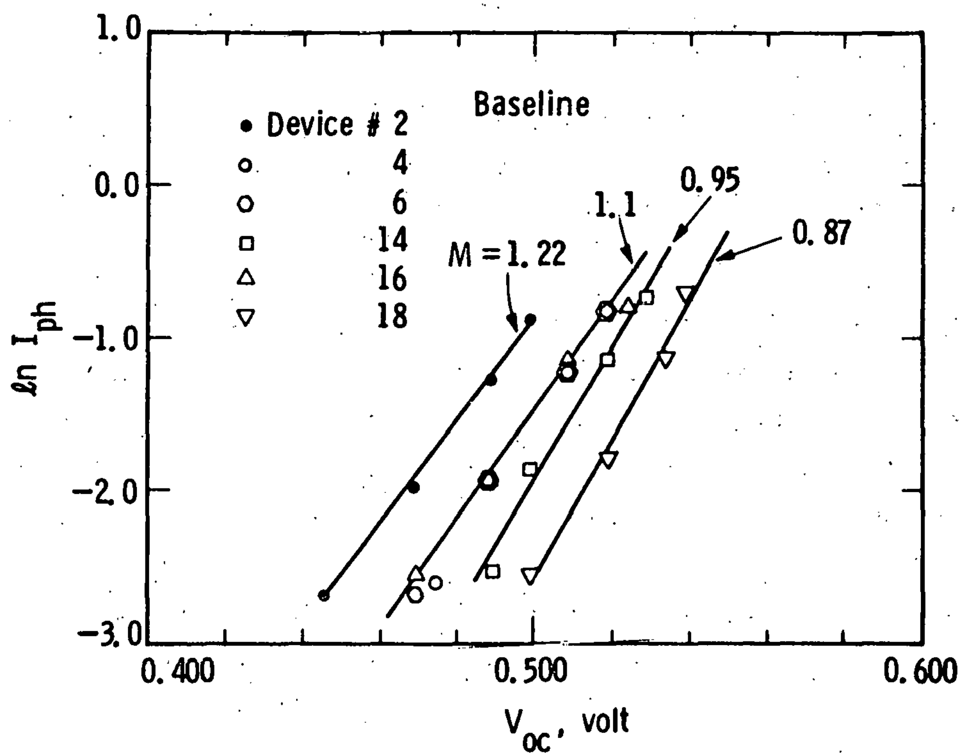

Figure 21 Illuminated current-voltage behavior (ln I_{ph} vs. V_{oc}) of six small MIS cells in base-line Ti-CZ polysilicon

Curve 731705-A

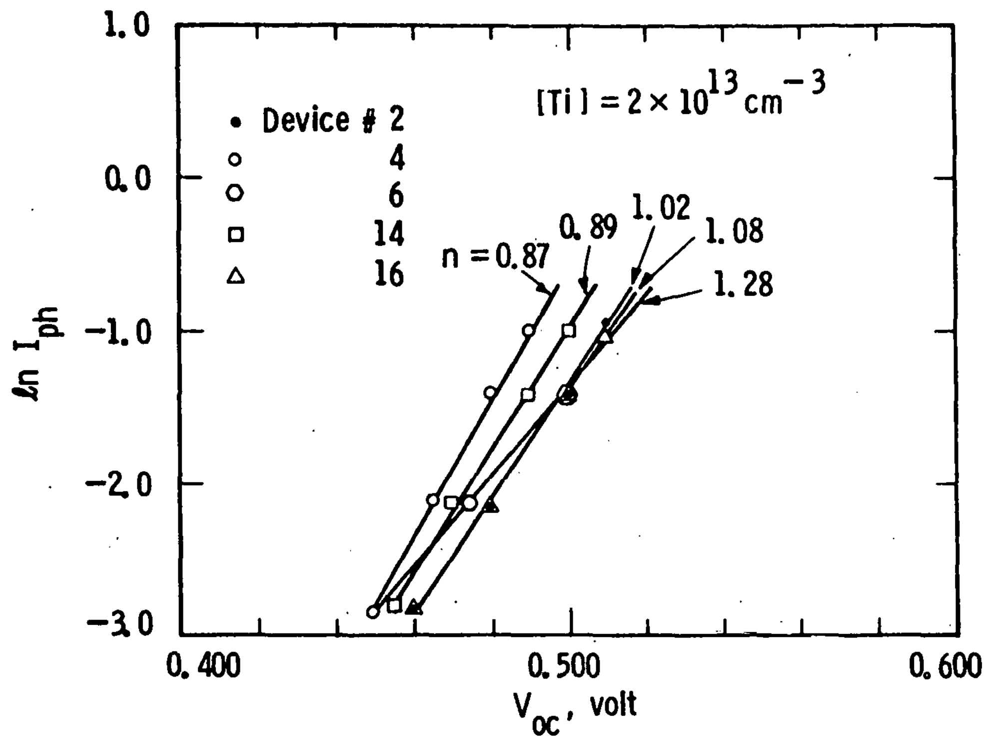

Figure 22 Illuminated current-voltage behavior (ln I_{ph} vs. V_{oc}) of five small MIS cells in CZ polysilicon doped with 2×10^{13} cm^{-3} Ti

With diffused junctions in this material, both Ti-doping and junction processing can produce a decrease in minority-carrier lifetime. Furthermore, the two mechanisms can be interactive. In this regard, MIS cell processing of Ti-doped CZ polycrystalline silicon allows for more direct, simpler interpretation of the effect of Ti.

Results for MIS cells in CZ polysilicon doped with $\sim 1 \times 10^{14}$ cm^{-3} Ti are shown in Fig. 23. As before, both I_{ph} and V_{oc} are lower for increased Ti-doping level. However, this case is more complex than the previous two. The decrease in I_{ph} for increasing Ti doping -- from 2×10^{13} cm^{-3} to 1×10^{14} cm^{-3} -- is fortuitously about the same as that observed for increasing the deliberate Ti-doping level from 0 to 2×10^{13} cm^{-3}. However, the corresponding decrease in V_{oc} at any fixed illumination level from 0.5 to 3 suns is significantly larger for increasing Ti concentration from 2×10^{13} cm^{-3} to 1×10^{14} cm^{-3} than for a deliberate increase from 0 to 2×10^{13} cm^{-3}. Also, diode ideality factors in this case are tightly distributed about $n = 1.3$, which is larger than for the previous two cases. Some of the decrease in V_{oc} is attributed to the fact that Ti is an effective lifetime killer in silicon, resulting in an increase in the diffusion component of diode opposing current. Also, at large Ti-doping levels ($\gtrsim 10^{14}$ cm^{-3}), the recombination component of diode opposing current approaches the diffusion component, resulting in additional V_{oc} reduction. The foregoing results for MIS cells in Ti-doped CZ polysilicon are summarized in Fig. 24. Individual data points were obtained by simple averaging of I_{ph} and V_{oc} for each level of Ti doping and light intensity.

We have previously experienced some difficulties with sample breakage during processing and handling of very thin (50 μm and 150 μm) polycrystalline silicon slices. We have developed and verified procedures for both high-temperature processing of diffused junction barriers (850°C) and of back-surface field regions (960°C), which minimize wafer breakage. We have also developed and verified mechanical handling

Curve 731702-A

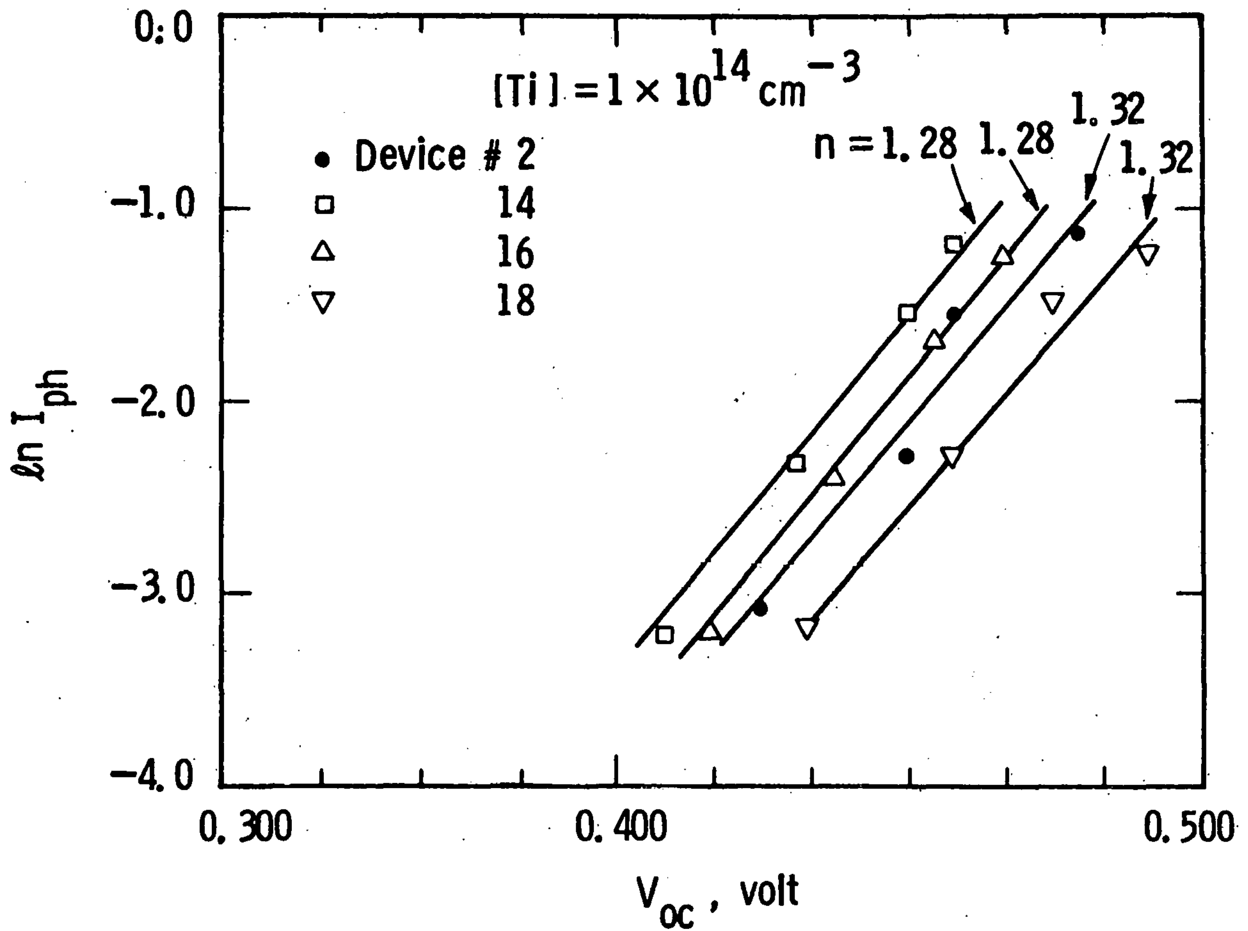

Figure 23 Illuminated current-voltage behavior (ln I_{ph} vs. V_{oc}) of MIS cells in CZ polysilicon doped with 1×10^{14} cm^{-3} Ti

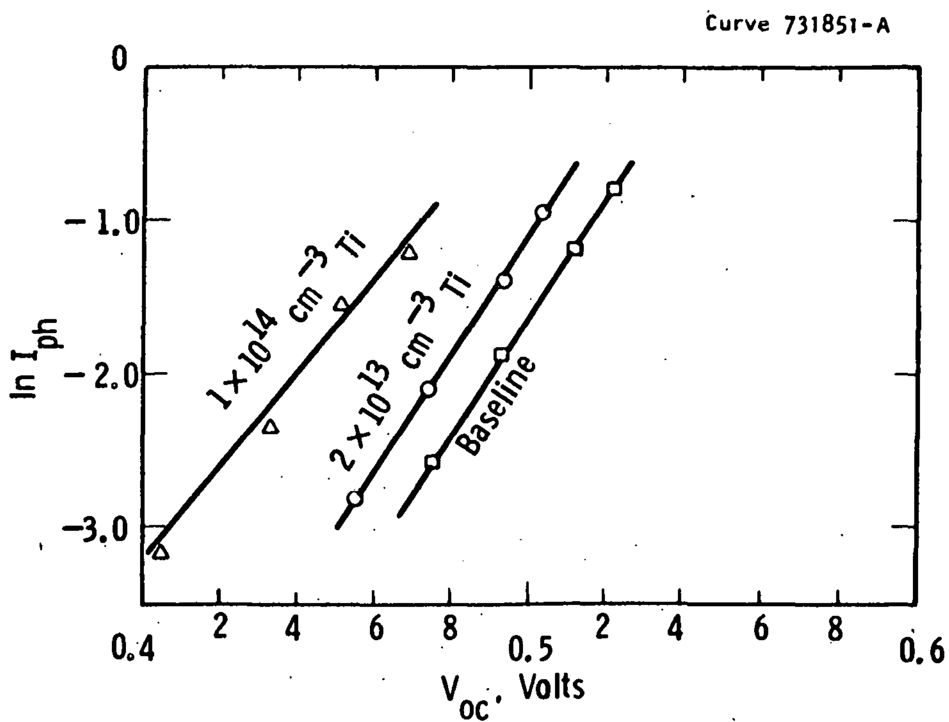

Figure 24 Illuminated current-voltage behavior (ln I_{ph}^{avg} vs. V_{oc}^{avg}) averaged for a number of MIS cells in base-line, 2×10^{13} cm^{-3}, and 1×10^{14} cm^{-3} Ti-doped material

procedures to minimize sample breakage, particularly during photolithographic processing. Matrix experiments involving comparisons of diffused junctions and MIS solar cells in thinned (50 μm and 150 μm) correlated Wacker SILSO and CZ polysilicon with and without deliberate titanium doping are underway. Sample processing will incorporate the refinements discussed above.

REFERENCES

1. C. H. Seager and D. S. Ginley, Appl. Phys. Lett. 52, p. 1050 (1981).
2. David Redfield, Appl. Phys. Lett. 38, p. 174 (1981).
3. B. W. Faughnan et al., "Thin Film Polycrystalline Silicon Solar Cells," Third Quarterly Report, Subcontract No. XS9-8276-1 (August 1980).
4. C. H. Seager, D. S. Ginley and J. D. Zook, Appl. Phys. Lett. 36, p. 831 (1980).
5. J. R. Szedon, Polycrystalline Silicon Contractors' Review Meeting, October 1978.
6. J. R. Szedon, T. A. Temofonte, et al., "Heterostructure Single Crystal Silicon Photovoltaic Solar Cells," Final Report, Contract No. AC-03-76ET-20408 (July 31, 1979).
7. J. R. Szedon, T. A. Temofonte, and T. W. O'Keeffe, Solar Cells, Vol. 1, p. 251 (1979/1980).
8. T. A. Temofonte, J. R. Szedon, et al., "Photovoltaic Mechanisms in Polycrystalline Thin Film Silicon Solar Cells," Final Report, Contract No. AC-01-79ET-23106 (February 16, 1981).
9. C. H. Seager and D. S. Ginley, Sandia Report,(August 1980).
10. P. H. Robinson and R. V. D'Aiello, Appl. Phys. Lett., 39, p. 63 (1981).
11. J. F. Wagner and C. W. Wilmsen, J. Appl. Phys., Vol. 50, p. 874 (1979).
12. C. R. Helms, Y. E. Strausser, and W. E. Spicer, Appl. Phys. Lett., Vol. 33, p. 767 (1978).
13. P. Morgen, J. H. Onsgaard, and S. Tougaard, Appl. Phys. Lett., Vol. 34, p. 446 (1980).

REFERENCES (Continued)

14. Steven R. Jost and Walter C. Johnson, Appl. Phys. Lett., Vol. 36, p. 446 (1980).

15. D. Redfield, Third Quarterly Progress Report, Contract No. AC-01-79-ET-23108 (May 1980).

16. D. Redfield, Proc. Fifteenth IEEE Photovoltaic Specialists Conf., 1179, IEEE Cat. No. 81CH1644-4 (1981).

17. D. Redfield, private communication.

18. Michael Spencer, D. K. Wagner, and L. F. Eastman, "Characterization of Grain Boundaries Using DLTS," 14th IEEE Photovoltaics Specialists Conference, 1140 (1980).

19. R. H. Hopkins, et al., Phase III Summary and 17th Quarterly Report, January 1980, on JPL Contract #954331.

ACKNOWLEDGMENTS

We appreciate the technical support of P. E. Barbarich, B. Blankenship, S. Karako, and G. S. Kostyak. We are very grateful to A. J. Noreika for the Auger measurements, to R. A. Hoffman for assistance in film preparation, to W. J. Biter for hydrogen passivation, and to A. J. Rohatgi for discussions and DLTS measurements. We thank K. B. Haun for typing the manuscript and G. S. Law for editing and producing the report.

☆U.S. GOVERNMENT PRINTING OFFICE: 1982-546-085/3076